Nuclear Physics B162 (1980) 397–439
© North-Holland Publishing Company

# PERTURBATIVE QCD IN A COVARIANT GAUGE

Ashton B. CARTER * and C.H. LLEWELLYN SMITH
*Department of Theoretical Physics, 1 Keble Road, Oxford OX1 3 NP, UK*

Received 9 July 1979

We present detailed calculations of the moments of structure functions, performed explicitly in a covariant gauge starting from familiar techniques. The results illustrate the central features of perturbative QCD (universal factorization of mass singularities, ladderization, etc.) and provide insight into their origin.

## 1. Introduction

In the last two years QCD has been shown to support a parton-like picture of certain hard scattering processes. The damping of large momentum transfers, due to the decrease of the running coupling constant $\bar{g}$, is just sufficient to ensure that the parton-model diagrams dominate to leading order in $\bar{g}^2$. Furthermore corrections can be calculated in a systematic expansion in powers of $\bar{g}^2$.

Given a large momentum scale $Q$ we can always use the coupling constant $\bar{g}(Q)$, but this is not enough to justify the use of perturbation theory. Technically a measurable quantity $W$ generally depends on masses ($m$), as well as any other dynamical variables ($Q'$) involved, i.e., $W = W(\bar{g}(Q), Q/m, Q/Q')$. If we attempt to expand $W$ in powers of $\bar{g}$ for large $Q$ we may find powers of $\ln(Q/m)$ which spoil the expansion (it may also be spoiled by powers of $\ln(Q/Q')$ if $Q/Q'$ is not held fixed when $Q$ is made large). Physically, sensitivity to $m$ indicates that the large-distance behaviour of the theory is involved, which we cannot possibly treat perturbatively. Therefore the use of perturbation theory requires either that $\ln(Q/m)$ terms do not occur (an example of such a mass finite case is $\sigma_{\mathrm{ee}}^{\mathrm{tot}}$) or that the logs can be summed up and the sensitivity to $m$ can somehow be factored out.

This "factorization" occurs in deep inelastic scattering where the operator product expansion (OPE) implies that the moments of the structure functions ** $W_n$

---

* Address after September 1: Physics Department, Rockefeller University, New York 10021, USA.

** In our explicit calculations we consider $W_n = \int x^n F_1(x, Q^2)\, \mathrm{d}x \simeq \int (x^{n-1} F_2/2)\, \mathrm{d}x$ to leading order in $\bar{g}^2$.

satisfy

$$W_n\left(g, \frac{Q^2}{m^2}, \frac{Q^2}{\mu^2}\right) = \sum_{i=1}^{N} C_i^n\left(g, \frac{Q^2}{\mu^2}\right) M_i^n\left(g, \frac{m^2}{\mu^2}\right) + \mathrm{O}\left(\frac{m^2}{Q^2}\right) , \tag{1.1}$$

where $\mu$ is the arbitrary scale chosen to define the coupling constant $g$. Because $\mu$ is arbitrary *

$$\mu^2 \frac{\mathrm{d}W_n}{\mathrm{d}\mu^2} = \left(\mu^2 \frac{\partial}{\partial\mu^2} + \mu^2 \frac{\partial g}{\partial\mu^2}\frac{\partial}{\partial g}\right) W_n = 0 .$$

In the non-singlet (NS) case (in which $N = 1$ in (1.1)) this leads immediately to the renormalization group equations ** (RGE) for $C^n$ and $M^n$, the anomalous dimensions being separation constants of the differential equation. The RGE allow us to sum up the logs of $Q^2/\mu^2$ and obtain the behaviour of the $C^n$ for large $Q^2$ in asymptotically free theories.

The separation into a calculable $Q^2$ dependent factor ($C^n$), determined by the short-distance properties of the theory, and an incalculable long-distance factor ($M^n$) can be put into closer correspondence with the parton picture by introducing another large scale $M$ and setting $\mu^2 = Q^2$:

$$\begin{aligned} W_n^{\mathrm{NS}}(Q^2) &= C_{\mathrm{NS}}^n(g, Q^2/\mu^2)[C_{\mathrm{NS}}^n(g, M^2/\mu^2)]^{-1} W_n^{\mathrm{NS}}(M^2) \\ &= C_{\mathrm{NS}}^n(\bar{g}(Q^2))\{[C_{\mathrm{NS}}^n(\bar{g}(Q^2), M^2/Q^2)]^{-1} W_n^{\mathrm{NS}}(M^2)\} . \end{aligned} \tag{1.2}$$

The first factor ($C^n$) represents the "hard scattering cross section", while the second $(C^n)^{-1} W_n$ is the "$Q^2$ dependent quark distribution", with calculable $Q^2$ dependence but unknown magnitude. (In the singlet ($N = 2$) case we need to consider simultaneously the function $\tilde{W}_n$, which would be measured by currents coupled to gluons; we then obtain coupled RGE and a description in terms of quark and gluon distributions.)

Recent progress has consisted of two closely linked parts:

(i) analysis of the diagrams summed up by the RGE, leading to information about the topology of the final states (jets, etc.) which is beyond the scope of the OPE;

(ii) the demonstration that factorization occurs in other hard processes (e.g., heavy $\mu$ pair production and large-$p_{\mathrm{T}}$ hadronic processes), the same "universal" $M^n$ occurring in each case. Likewise in production processes ($e^+e^- \rightarrow \pi + ...$, etc.) there is factorization and the long-distance part is universal.

In this paper we present calculations in the leading log approximation (LLA) which support the idea of universal factorization, and, we feel, give insight into the structure of the theory. An outline of our approach was published some time ago [1]. It turned out that very similar conclusions had been reached independently by Dokshiter et al. [2], who (like us) were inspired by the classic work of Gribov and Lipatov [3], and by others [4], many of whom were inspired by the important papers of Sterman and Weinberg [5], on mass finite quantities, and of Politzer [6], who stressed the notion of factorization of mass singularities. Subsequently factorization has been proved for non-leading logs [7]. Nevertheless we feel that we have something to add for several reasons.

---

* If the quark mass parameters $m$ are defined at $\mu$ there should also be a $\mu^2(\partial m/\partial\mu^2)\ \partial/\partial m_{\mathrm{q}}$ term but this contributes to terms of order $m^2/Q^2$ in (1.1), which we ignore.

** The relevant equations are collected in the appendix where we also define all the symbols employed in the text and figures.

(i) We work in a covariant gauge in which we can calculate explicitly. In contrast, other authors have mostly employed general arguments and used axial gauges, which makes it hard to check the conclusions. In fact, ours is the first fully explicit calculation of $W_n$ beyond $O(g^2)$ in any gauge as far as we know. (The pioneering work of Gribov and Lipatov was done in the Feynman gauge, but they considered an abelian model which is much less complicated than QCD; furthermore we believe that we are not alone in having found their paper very hard to understand.)

(ii) Our calculations start from familiar diagrammatic techniques and therefore offer considerable heuristic value. The physics is made clear: one sees the infrared and "Kinoshita-Lee-Nauenberg" (KLN) cancellations [8] occur line by line and the workings of gauge invariance to eliminate singularities associated with spurious (gauge) degrees of freedom.

We consider as a paradigm the specific case of $W_n$ for deep inelastic scattering (it should be clear that the technique can easily be applied to other hard processes). Our goal is to rederive the well-known result that

$$W_n^{\mathrm{NS}}(Q^2) = \left[\frac{\bar{g}^2(Q^2)}{\bar{g}^2(M^2)}\right]^{2\gamma_{n-1}^{\mathrm{NS}}/g^2\beta_0} W_n^{\mathrm{NS}}(M^2) \tag{1.3}$$

in LLA and the corresponding singlet result (the symbols are all defined in the appendix). For a given power $(g^2)^n$ we identify the leading powers of $\ln(Q^2/\mu^2)$, $\ln(Q^2/m^2)$ and $\ln(m^2/\mu^2)$ and then sum over $n$ (some terms can be constructed from others, using the fact that $W_n$ must be $\mu$-independent, but we prefer to identify their origin explicitly).

There are four possible sources of logs:

(i) ultraviolet logs, due to the dressing of vertices and propagators and to wave-function renormalization (these logs introduce $\mu$-dependence);

(ii) logs due to collinear radiation of *real* particles (which depend on $m$);

(iii) "parallel logs" due to *virtual* collinear emission and absorption of almost real particles (these also depend on $m$);

(iv) logs left over after the cancellation of infrared divergences between real and virtual processes involving soft particles (in fact we shall show that such logs are absent).

If we consider the virtual forward Compton amplitude $T$ (recall that structure functions $W \propto \mathrm{Im}\, T$), it turns out that intermediate $N$-particle states in the $t$-channel only give rise to mass singularities (giving logs of types (ii) and (iii)) if $N - 2$ of the particles are longitudinal gluons, with $\epsilon_\mu(k) \propto k_\mu$ (this is easily made plausible by dimensional arguments [7]; we shall see it explicitly). It is clear that the contributions of these longitudinal gluons are in some sense artificial. Mass singularities are associated with the propagation of real intermediate states [9], i.e., virtual processes which could become real as $m \to 0$, allowing the vertices to separate by arbitrary distances. Longitudinal gluons are unphysical and cannot contribute to genuine real processes. Therefore, if we sum over all diagrams, their contributions must cancel.

In the axial gauge the propagators of longitudinal gluons have no poles as $k^2 \to 0$ (and correspondingly there are no ghosts). Therefore, only states with $N = 2$ give singularities diagram by diagram ("ladderization"). The price to be paid for this simplification is that there are additional (spurious) poles in the propagators and explicit calculations are very difficult.

Insofar as *real* radiation is concerned, we can reproduce this simplification (*regardless* of our choice of gauge) merely by summing over physical, transverse polarization states for real gluons. We sum up the effects of *virtual* (longitudinal) gluons using Ward identities, which express the fact that contributions of longitudinal gluons must be gauge artifacts, since they are not associated with a physical pole.

Covariant gauges are generally characterized by a parameter $\alpha$ such that the gluon propagator $D_{\mu\nu}$ satisfies

$$k^2 D_{\mu\nu}(k^2)\big|_{k^2=-\mu^2} = -\alpha g_{\mu\nu} + (1-\alpha)\left(-g_{\mu\nu} + \frac{k_\mu k_\nu}{k^2}\right) .$$

It turns out that (as discussed in detail in sect. 3) the $k_\mu k_\nu/k^2$ term gives rise to problems in our approach. They cannot be avoided by choosing $\alpha = 1$ since the $k_\mu k_\nu$ term is induced by radiative corrections for $k^2 \neq -\mu^2$. However, it is possible [10] to let $\alpha$ be a function of $k^2$ such that

$$k^2 D_{\mu\nu}(k^2) = -\alpha(k^2)\, g_{\mu\nu} . \tag{1.4}$$

We call this choice "stagnant Feynman gauge" (SFG). In SFG the usual renormalization group equations hold, but without the "gauge drift" term $\delta\partial/\partial\alpha$ and with $\beta(g)$ and the $\gamma(g)$'s calculated in SFG (this is the same as calculating them in the Feynman gauge to the order considered in this paper).

This paper is organised as follows. In sect. 2 we discuss the calculation of $W_n$ to $O(g^2)$ in detail in order to develop calculational techniques which can be used in higher orders. In sect. 3 we calculate $W^{\mathrm{NS}}$ to $O(g^4)$; this is enough to understand essentially all the physics of asymptotic freedom and mass singularities. In sect. 4 we present the Ward identities and use them to sum up the effects of "parallel logs" to all orders. The summation of all contributions to all orders (in LLA) and factorization using a large scale $M$ are discussed in sect. 5. Sect. 6 is devoted to mixing and the singlet case. In sect. 7 we comment on the extension to non-leading logs and applications to other process.

## 2. Order $g^2$

In this section we discuss the leading logarithmic contributions to $W_n$ in $O(g^2)$ introducing techniques needed in higher orders. Although the non-abelian couplings are not yet evident, much of the essential physics appears already in this order. At the end we shall display the features which persist in higher orders. Initially we shall encounter infrared singularities as formally divergent integrals. We discuss the regularization of these integrals and their combination into an infrared-finite result when all the ingredients are assembled.

With $m = 0$ the amplitudes of figs. 1a,b would be singular as $t \to 0$ and as $s \to 0$ ($x = Q^2/(2p \cdot q) \to 1$) respectively, since at these points the exchanged quarks become real and the propagators blow up. Provided we only consider *physical gluons with transverse polarizations*, the vertex in fig. 1a is proportional to $\sqrt{-t}$, because the quark-gluon vertex conserves helicity (to order $m^2$) and emission of a transverse gluon is forbidden as $\theta \to 0$ ($t \to 0$). This means that for $x \neq 1$ the divergence in $W$ comes from the square of fig. 1a only and is logarithmic (the additional singularity as $x \to 1$ coincides with an infrared divergence as discussed below). We can find the coefficient of this singularity by extracting the $(-t)^{1/2}$ factor from the amplitude and ignoring all terms of higher power in $t$. Thus, dropping all terms which do not contribute to the logarithmic singularity as $m \to 0$, the squared matrix element (summed/averaged over spins and colours) is

$$M_a = (ig)^2 C_F \sum_{\text{physical } \epsilon} \mathrm{Tr}\, \not{p} \frac{\not{\epsilon}(\not{p} - \not{k})}{-t + m^2} M^0 \frac{(\not{p} - \not{k}) \not{\epsilon}}{-t + m^2}$$

$$= (ig)^2 C_F \left(\frac{1}{-t + m^2}\right)^2 \sum_{\epsilon} \mathrm{Tr}\{(2\epsilon \cdot p)^2 (\not{p} - \not{k}) - t\not{k} + O(-t)^{3/2})\} M^0$$

$$\simeq g^2 C_F \frac{-2}{-t + m^2} \frac{1 + y^2}{y(1 - y)} \mathrm{Tr}(\not{p} - \not{k}) M^0 , \qquad (2.1)$$

where (i) we assume $Q^2 >> m^2$ and work in the frame $q^0 = 0$ in which the momenta are large: $2E \simeq 2|\boldsymbol{p}| = \sqrt{Q^2}/x$; (ii) we can therefore set $k_\mu = (1 - y) P_\mu + O(\sqrt{t})$ for $y \neq 1$; (iii) the gluon polarizations are spatial and transverse: $\epsilon^0 = 0$, $\boldsymbol{\epsilon} \cdot \boldsymbol{p} = |\boldsymbol{p}| \sin\theta \simeq -t/|\boldsymbol{k}|$; (iv) $\mathrm{Tr}(\not{p} - \not{k}) M_0$ is the squared matrix element for a real incom-

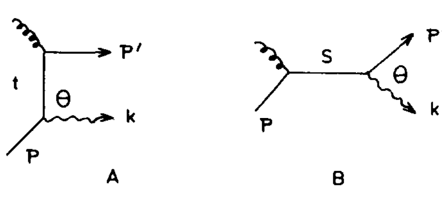

Fig. 1.

ing quark with momentum fraction

$$x' \equiv \frac{Q^2}{2q\cdot(p-k)} \simeq \frac{x}{y}$$

in our leading log approximation. In this configuration the gluon phase space simplifies to

$$\frac{d^3k}{2k(2\pi)^3} \simeq \frac{1}{16\pi^2}\, dy\, d(-t)\,,$$

so that finally we obtain

$$W_a(x) = \lambda\, C_F \ln\frac{Q^2}{m^2} \int_0^1 dy \frac{1+y^2}{y(1-y)}\, W^0(x')\,, \tag{2.2}$$

with $\lambda \equiv g^2/8\pi^2$, where the log arises from the $t$ integral. Taking moments,

$$W_n^a \equiv \int_0^1 x^n W_a(x)\, dx = \lambda\, C_F \ln\frac{Q^2}{m^2}\left[\int_0^1 dy\, y^n \frac{1+y^2}{1-y}\right] W_n^0\,. \tag{2.3}$$

The singularity as $y \to 1$ reflects the infrared divergence as $|\boldsymbol{k}| \to 0$ and will be dealt with below. Eq. (2.2) clearly generalises to the more complicated process shown in fig. 2, with $W^0(x')$ replaced by the probability corresponding to the process quark + photon → X induced by a quark with momentum $yp$.

Similarly, we can extract the log contributed by the square of the amplitude of fig. 1b by noting that in our frame, as $s \to m^2$ $(x \to 1)$, $\boldsymbol{p}'$ becomes parallel to $\boldsymbol{k}$, so that we can set $k_\mu = (1-y)(q_\mu + p_\mu)$ after we have extracted a $\sqrt{s}$ "helicity conservation" factor. Thus fig. 1b gives:

$$M_b \simeq g^2\, C_F \frac{2}{s-m^2}\frac{1+y^2}{1-y}\, \mathrm{Tr}(\not{p}' + \not{k})\, \not{\epsilon}_\gamma \not{p} \not{\epsilon}_\gamma\,. \tag{2.4}$$

Introducing the identity

$$1 = \delta^4(p+q-l)\, d^4l\, \delta(l^2 - s)\, ds\,,$$

the phase-space factor is proportional to

$$\delta^4(p+q-l)\, d^4l\, \delta(l^2-s)\, dy\, ds$$

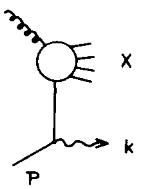

Fig. 2.

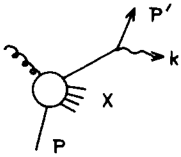

Fig. 3.

in the $p' \parallel k$ configuration. Hence we obtain

$$W_b(x) \simeq \lambda\, C_F \int dy \int \frac{ds}{s - m^2}\, \frac{1 + y^2}{1 - y} \left[\tfrac{1}{2}\delta(1 - x + \frac{(s - m^2)\,x}{Q^2}\right], \tag{2.5}$$

where the last factor would be just $W_0(x)$ for $s = m^2$. In fact, since we only want the $x$-moments, we can replace (2.5) by

$$W_b(x) \simeq \lambda\, C_F \ln \frac{Q^2}{m^2} \left[\int_0^1 dy\, \frac{1 + y^2}{1 - y}\right] W_0(x) \tag{2.6}$$

in LLA if we realize that the $s$-integral converges for $y \neq 1$ since $ys > (1 - y)\, m^2$ (the infrared divergence is discussed below). It should be clear that in LLA the contribution of the process of fig. 3 is given by eq. (2.6) with $W_0(x)$ replaced by the probability corresponding to the process quark + photon → X + quark and $Q^2$ replaced in the logarithm by some suitable scale set by the process within the circle.

The interference of amplitudes 1a and 1b does not contribute to leading logs if the emitted gluon is transverse *. The implications of this important point are discussed further below.

Fig. 4 contains both mass singularities and an ultraviolet divergence. Since we perform the vertex renormalization off-mass-shell, the two kinds of divergence are easy to separate. The mass singularities correspond to real subprocesses, where internal particles propagate on their mass-shells and the vertices can separate to arbitrarily large distances in coordinate space in the $m = 0$ limit. For fig. 4 there are two distinct possibilities (modulo the infrared region which we discuss below): $k^2 = 0$ with $k^0 > 0$ and either (i) $(p - k)^2 \simeq 0, p^0 - k^0 > 0$ or (ii) $(p' - k)^2 \simeq 0, p'^0 - k^0 > 0$. In order to see this, parametrize the loop as follows **:

$$k_\mu = z(xp_\mu + q_\mu) + (1 - y)\, p_\mu + k^t_\mu\,, \tag{2.7}$$

---

[*] If we included the (spurious) contributions of scalar and longitudinal gluons (which cancel) by using $\Sigma\epsilon^*_\mu\epsilon_\nu = -g_{\mu\nu}$, the helicity argument would break down and the interference term between 1a and 1b would also give a log.

[**] The choice of the projection vector given by the first term on the right-hand side of (2.7) is more or less arbitrary. One merely requires that its square be of $O(m^2)$ and its contraction with $p_\mu$ be large and positive.

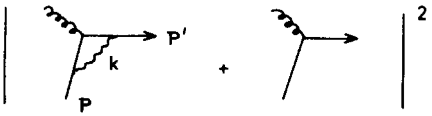

Fig. 4.

choosing $k^t_\mu$ such that $k^t \cdot p = k^t \cdot (xp + q) = 0$ and $k^t \cdot k^t = -k_t^2$. Then focusing upon the propagators contributing to possibility (i) above and setting $m = 0$ for the moment,

$$\frac{d^4k}{(k^2 + i\epsilon)((p - k)^2 + i\epsilon)} = \frac{2\pi\nu \, dz \, d(1 - y) \, dk_t^2}{(2\nu z(1 - y) - k_t^2 + i\epsilon)(2\nu zy - k_t^2 + i\epsilon)} , \tag{2.8}$$

where $\nu \equiv p \cdot q$. The integral is zero unless the integrand has poles in both the upper half complex $z$-plane and the lower half $z$-plane; thus $y$ and $y - 1$ have opposite signs, i.e., $0 \leqslant y \leqslant 1$, corresponding to $k^0 \geqslant 0, p^0 - k^0 \geqslant 0$. No matter which plane we close the integration contour in, corresponding to putting one or the other propagator on-shell, the residue is proportional to $1/k_t^2$, and the log comes from integration of this variable over an asymptotic range bounded above by $Q^2$ and below (reinstating the quark mass) by $m^2$.

Since $z \sim k_t^2$ in the vicinity of either pole, all terms of $O(z)$ or $O(k_t^2)$ are neglectable in LLA; in the numerator, we can set $k_\mu = (1 - y) p_\mu$. Thus at the incoming end of the numerator spinor chain we can write

$$\cdots (\not{p} - \not{k} - m) \gamma_\mu u(p) \simeq \cdots \frac{2y}{1 - y} k_\mu u(p) . \tag{2.9}$$

This means that the virtual gluons responsible for the logarithmic divergence are *longitudinally polarized* ($\epsilon_\mu \sim k_\mu$). When this gluon is attached to the other end of the spinor chain, we get

$$\bar{u}(p') \gamma_\mu \frac{1}{\not{p}' - \not{k} - m} \cdots k^\mu = \bar{u}(p') [(\not{p}' - m) - (\not{p}' - \not{k} - m)] \frac{1}{\not{p}' - \not{k} - m} \cdots$$

$$= -\bar{u}(p') \cdots ,$$

so that to LLA the amplitude is proportional to the Born amplitude. This is the first primitive example of the use of a Ward identity to treat longitudinal gluons.

Finally, then, the contribution of fig. 4 corresponding to $k \mathbin{/\!/} p$ (the first possibility) is:

$$W_n^{k/\!/p} = \int_{m^2}^{Q^2} \frac{dk_t^2}{k_t^2} \frac{g^2}{8\pi^2} C_F \left[ \int_0^1 dy \frac{-2y}{1 - y} \right] W_n^0 = \lambda \, C_F \ln \frac{Q^2}{m^2} \left[ \int_0^1 dy \frac{-2y}{1 - y} \right] W_n^0 .$$

An identical contribution is similarly obtained from the $k \,/\!\!/\, p'$ region:

$$W_n^{k/\!\!/p'} = \lambda\, C_{\mathrm{F}} \ln \frac{Q^2}{m^2} \left[ \int_0^1 \mathrm{d}y \, \frac{-2y}{1-y} \right] W_n^0 \,. \tag{2.10}$$

We pause now to consider the problem of soft (infrared) divergences. Adding eqs. (2.3), (2.9) and (2.6), (2.10), we see that the divergences as $y \to 1$ cancel separately in the $k \,/\!\!/\, p$ and $k \,/\!\!/\, p'$ regions, and this naive procedure actually gives the correct answer:

$$W_n^{(2.3)+(2.9)} = \lambda\, C_{\mathrm{F}} \ln \frac{Q^2}{m^2} \left[ \int_0^1 \mathrm{d}y \, \frac{y^n(1+y^2) - 2y}{1-y} \right] W_n^0$$

$$= \lambda\, C_{\mathrm{F}} (f_n + \tfrac{1}{2}) \ln \frac{Q^2}{m^2} W_n^0 \,, \tag{2.11}$$

$$W_n^{(2.6)+(2.10)} = \lambda\, C_{\mathrm{F}} \ln \frac{Q^2}{m^2} \left[ \int_0^1 \mathrm{d}y \, \frac{(1+y^2) - 2y}{1-y} \right] W_n^0$$

$$= \lambda\, C_{\mathrm{F}} (\tfrac{1}{2}) \ln \frac{Q^2}{m^2} W_n^0 \,, \tag{2.12}$$

(where $f_n$, which is defined in the appendix, is proportional to the familiar non-singlet anomalous dimension of the operator product expansion). We shall now show that when we combine real and virtual contributions the region $k < \delta\sqrt{Q^2}$ ($k = |\boldsymbol{k}|$) contributes terms of order $\delta \ln(Q^2/m^2)$ (where $\delta$ is arbitrarily small but fixed as $Q^2 \to \infty$). We can therefore exclude the region $y > 1 - \delta$ and the region where $k$ is small but $\theta$ is large (which we have ignored altogether). It follows that (2.11) and (2.12) are correct.

Infrared divergences are most easily treated by (temporarily) using $\Sigma \epsilon_\mu^* \epsilon_\nu = -g_{\mu\nu}$, in which case it is well-known that there is a direct topological correspondence between real and virtual contributions which combine to give finite answers. Treating them in turn:

(i) $|$fig. 1b$|^2$ + ($p'$ wave-function renormalization to elastic scattering) is finite. The divergent contribution of fig. 1b is

$$\sum_{\epsilon'} \int \frac{\mathrm{d}^3 k}{k} \left( \frac{\epsilon' \cdot p'}{p' \cdot k} \right)^2 = \int \frac{\mathrm{d}k}{k} \int \frac{-m^2 \, \mathrm{d}\Omega_k}{(E' - p' \cos\theta)^2} \,.$$

The first factor behaves as $(Q^2)^\epsilon/\epsilon$ if we go to $4 + 2\epsilon$ dimensions ($\epsilon > 0$). The angular integral would be linearly divergent if $m$ were zero, so the second factor is proportional to $m^2(1/m^2)(m^2/Q^2)^\epsilon$. The net result ($\sim (m^2)^\epsilon/\epsilon$) depends only on $m^2$, as we might expect for incoherent radiation from an external line, and cancels the divergent contribution to wave-function renormalization.

(ii) Likewise $|\text{fig. 1a}|^2$ + ($p$ wave-function renormalization to elastic scattering) is finite and does not leave a $\ln(Q^2/m^2)$ factor as might have been feared.

(iii) The interference of figs. 1a and 1b + fig. 9 is finite. As usual the $k$ and angular integrals factorize, the former giving $(Q^2)^\epsilon/\epsilon$. The angular integral is at most logarithmically divergent as $m \to 0$ so that in both the real (r) and virtual (v) cases it gives

$$A^{\mathrm{r,v}} + \frac{B^{\mathrm{r,v}}}{\epsilon}\left[\left(\frac{m^2}{Q^2}\right)^\epsilon - 1\right], \tag{2.13}$$

but it cannot generate terms $\sim(m^2/Q^2)^\epsilon$ (which could only come from $m^2$ times an integral which is linearly divergent as $m \to 0$). The sum of real and virtual contributions is infrared finite, which requires that separately

$$B^{\mathrm{r}} + B^{\mathrm{v}} = 0$$

(to eliminate terms $\sim\epsilon^{-1}\ln(Q^2/m^2)$) and

$$A^{\mathrm{r}} + A^{\mathrm{v}} = 0$$

(to eliminate $\epsilon^{-1}$), with the result that no $\ln(Q^2/m^2)$ terms remain.

It follows that the region $k < \delta\sqrt{Q^2}$ contributes terms of $O(\delta) + O(\delta\ln(Q^2/m^2))$ (the latter being due to the usual parallel divergences unaccompanied by $k^{-1}$) and can be ignored. The same is true in the non-abelian case, including the effects of radiation from gluon lines, because real and virtual contributions still cancel between diagrams with related topologies [11]. Again wave-function renormalization plus incoherent radiation from external lines is finite and the cancellation does not leave logs since both behave as $(m^2)^\epsilon\epsilon^{-1}$. Virtual contributions combine with related interference terms to a finite result free of logs because both behave as $(Q^2)^\epsilon\epsilon^{-1}$ for the reason discussed above. We can therefore freely manipulate divergent $y$-integrals, which will combine into an infrared-finite result, and ignore the $k$ small, $\theta$ large region, as we have done above (thus it suffices to consider all gluons to be "hard").

Finally, we must include in $W_n$ the "ultraviolet" logarithm from the $k \to \infty$ region of the loop in fig. 4, which gives

$$W_n^{\mathrm{UV}} = -\lambda\, C_{\mathrm{F}} \ln\left(\frac{Q^2}{\mu^2}\right) W_n^0 \tag{2.14}$$

and the ultraviolet divergent contribution * of wave-function renormalization on each of the outgoing lines, given by the usual renormalization group anomalous dimension:

$$W_n^{\mathrm{ren}} = 2\left[-\tfrac{1}{2}\lambda\, C_{\mathrm{F}} \ln\left(\frac{\mu^2}{m^2}\right)\right] W_n^0\,. \tag{2.15}$$

---

* We ignore the infrared divergence in the renormalizations. They cancel against soft divergences in $|1\mathrm{a}|^2$ and $|1\mathrm{b}|^2$, as discussed above.

At last we add up all the contributions (eqs. (2.11), (2.12), (2.14), (2.15)) to $W_n$ in this order:

$$W_n^{\mathrm{O}(g^2)} = \lambda\, C_\mathrm{F}\, f_n \ln\left(\frac{Q^2}{m^2}\right) W_n^0 = -\gamma_{n-1}^{\mathrm{NS}} \ln\left(\frac{Q^2}{m^2}\right) W_n^0 \,. \tag{2.16}$$

To $\mathrm{O}(g^2)$ accuracy, then

$$\begin{aligned} W_n &= \left(1 - \gamma_{n-1}^{\mathrm{NS}} \ln\left(\frac{Q^2}{m^2}\right)\right) W_n^0 \\ &= \left(1 - \gamma_{n-1}^{\mathrm{NS}} \ln\left(\frac{Q^2}{\mu^2}\right)\right)\left(1 + \gamma_{n-1}^{\mathrm{NS}} \ln\left(\frac{m^2}{\mu^2}\right)\right) W_n^0 + \mathrm{O}(g^4)\,, \end{aligned} \tag{2.17}$$

which is written in the (trivially) factorized form of eq. (1.1) and satisfies to this order the appropriate renormalization group equation.

We now call attention to several important features of this calculation which persist in higher orders.

(i) With only physical (transverse) produced gluons interference terms such as those illustrated in fig. 5 never produce leading logs. This follows immediately from the "helicity" zeros which make the individual amplitudes behave as $\sqrt{s}/s$, $\sqrt{t}/t$ etc., when we approach the parallel configuration. Since these factors diverge in different regions of phase space, only symmetric diagrams (as in fig. 6) possess the required logarithmic singularities. The fact that interference terms do not contribute in LLA ("ladderization") allows a probability interpretation and accounts for the success of the parton model.

(ii) The leading logarithm comes from a wide (asymptotic) range of the logarithmic variable ($s$, $t$, etc.). We can truncate the integrals at either the upper or lower end and still obtain the leading log asymptotically, e.g.,

$$\int_{m^2}^{Q^2} \frac{\mathrm{d}|t|}{|t|} \overset{\mathrm{LL}}{=} \int_{m^2}^{\epsilon Q^2} \frac{\mathrm{d}|t|}{|t|} \overset{\mathrm{LL}}{=} \int_{m^2/\epsilon}^{Q^2} \frac{\mathrm{d}|t|}{|t|}\,, \tag{2.18}$$

where $\epsilon$ is arbitrarily small but fixed as $Q^2 \to \infty$. Nevertheless, the transverse momentum $\langle p_\mathrm{t}^2 \rangle \sim \langle |t| \rangle$ vanishes to this order of approximation, since the integral (2.18) is no longer logarithmic if any power of $t$ is added to the integrand. In this sense, it is the region of *small* logarithmic variables which gives the leading logs. This means all particles are emitted at small angles to the vectors $p$ and $p + q$ ($\theta \to 0$ in fig. 1), and

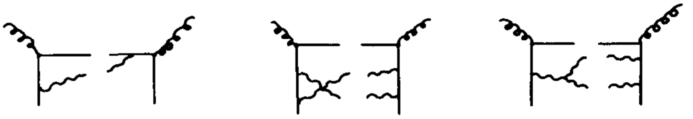

Fig. 5.

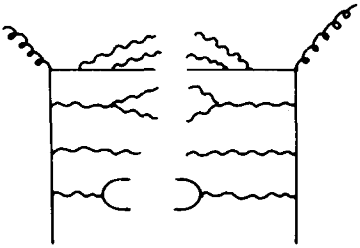

Fig. 6.

the final state has a two-jet structure. Thus in LLA we can treat the particles involved as highly virtual ($|t| >> m^2$), and use the asymptotic form for ultraviolet vertex and propagator corrections, yet almost real ($|t| << Q^2$) as far as kinematics is concerned.

(iii) The virtual gluons contributing parallel divergences are longitudinally polarized ($\epsilon_\mu \sim k_\mu$), and the amplitudes contributing these singularities can be summed up using Ward identities. The result is an "effective" emission diagram (see fig. 7) in which the divergence is collected on the external line. With this effective diagram is associated a factor

$$\lambda\, C_{\mathrm{F}} \left( \int_0^1 \mathrm{d}y \frac{-2y}{1-y} \right) \times \log\,, \tag{2.19}$$

as in (2.9) and (2.10).

(iv) Mass singularities associated with the outgoing quark (eqs. (2.6), (2.10), (2.15)) *cancel in the inclusive sum*, leaving a residual logarithm

$$\tfrac{1}{2}\lambda\, C_{\mathrm{F}} \ln\left(\frac{Q^2}{\mu^2}\right). \tag{2.20}$$

This cancellation is the realization, in this order, of the Kinoshita-Lee-Nauenberg (KLN) theorem. The log, (2.20), which remains is the ultraviolet renormalization appropriate to a quark propagating an amount $Q^2$ from its mass-shell. This is a general feature: there are never any mass divergences associated with outgoing (i.e., unobserved) lines, and the $\ln(\mu^2/m^2)$ terms associated with wave-function renormali-

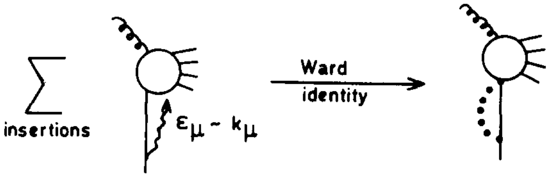

Fig. 7.

zation get turned into $\ln(\mu^2/M^2)$, where $M$ is the upper range set by the kinematics for the mass of the line and all particles emitted from it (in the LLA, there is no other scale). It is plausible (and we shall later show in detail) that the total effect of radiation (real and virtual) off unobserved lines, is given by the functions $Z_3$ and $Z_3^{\mathrm{F}}$ which multiply the bare propagators for very virtual massless quarks and gluons. (The functions $Z_3$ and $Z_3^{\mathrm{F}}$ can be calculated using the renormalization group).

(v) The soft region ($k < \delta\sqrt{Q^2}$) can be ignored completely. We can therefore freely manipulate apparently divergent $y$ integrals which combine to well-defined results, e.g., the $k \parallel p$ logs give

$$\frac{1+x^2}{1-x} - \delta(1-x)\int_0^1 \mathrm{d}y\left[\frac{1+y^2}{1-y} - \frac{1}{2}\right],$$

which is the Altarelli-Parisi distribution [12] apart from the final factor $(-\frac{1}{2})$. In higher orders it is always the finite moments of this combination which occur in $W_n$, whose $n$ dependence is determined from $f_n \sim \gamma_{n-1}^{\mathrm{NS}}$, as in eq. (2.11).

## 3. Order $g^4$

In this section we present explicitly the leading logs contributed by all $O(g^4)$ diagrams. This is enough to understand essentially all the physics of asymptotic freedom and mass singularities in QCD perturbation theory. After some preliminary remarks we shall discuss all of the various contributions (ultraviolet or parallel) of every diagram in turn. The results are given in a table enabling us to focus on the physics in the text. At various junctures, which we denote CC (for "collection and comment"), we shall pause to collect various contributions which combine together in a significant way, with an eye to features which generalize in higher orders. The complete result is assembled and discussed at the end.

Up to now we have treated massive on-shell quarks, but henceforth we set $m = 0$, taking incident quarks (and gluons, in the mixing case) slightly off-shell. It is also convenient to take the final particles slightly off-shell *. This is largely a bookkeeping device, regularizing and labelling parallel divergences at intermediate stages of the calculation and indicating how the KLN cancellations work. Since in reality (as discussed in sect. 5) we are provided with virtual initial quarks and gluons by a hadronic vertex which we cannot calculate, and in any case the notion of mass-shell is not sensible for confined quarks and gluons, it is really the structure functions for virtual particles which we require. Of course, off-shell quantities are not well-defined (e.g., they are gauge dependent). One is accustomed to thinking that the difference

---

* In principle the incident particles should be spacelike and the produced particles timelike to avoid spurious singularities. In practice these cause no trouble and we shall not bother to keep track of signs and distinguish, e.g., $\ln(Q^2/p^2)$ from $\ln(Q^2/-p^2)$.

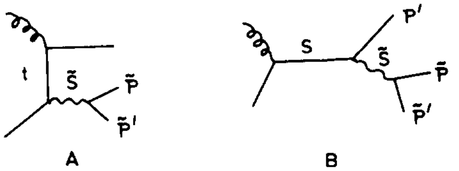

Fig. 8.

between on- and off-shell quantities must be of order $(p^2 - m^2)/Q^2$ and is therefore irrelevant at large $Q^2$. Happily, in our stagnant Feynman gauge this is true *diagram by diagram*, a circumstance which would *not* obtain in a general covariant gauge ★. We can therefore treat diagrams with off-shell particles, confident that our calculations continue smoothly onto the mass-shell, where their gauge invariance is assured.

Turning now to explicit evaluation of the $O(g^4)$ diagrams, we begin with the instructive and relatively simple case of $q\bar{q}$ production (fig. 8). These diagrams give double logs in the configuration $\tilde{p} \parallel \tilde{p}'$ ($(\tilde{p} + \tilde{p}')^2 \equiv \tilde{s} \simeq 0$) and $\tilde{p} + \tilde{p}'$ parallel to $p$ or $p'$ ($t \simeq 0$ or $s \simeq 0$). The amplitudes behave as $\tilde{s}^{-1/2}$ times $t^{-1/2}$ or $s^{-1/2}$ (from helicity conservation) so that (as in the case of figs. 1a and b),

*CC1*: we need not consider interference terms to obtain leading logs. Because the $q\bar{q}$ vertex conserves helicity the virtual gluon becomes transverse as $\tilde{p}$ and $\tilde{p}'$ become parallel. Thus it is clear that the contributions of figs. 8a and b are proportional to 1a and b, respectively.

*CC2*: In diagrams with the topology of fig. 8 (e.g., fig. 11 below) the singularities as $\tilde{s} \to 0$ are associated with the possibility of virtual processes becoming real. The

---

★ In other covariant gauges the $k_\mu k_\nu/(k^2)^2$ term in the propagator creates problems. These are illustrated by the amplitude of fig. 4. If we set $\not{k} = (\not{p} - m) - (\not{p} - \not{k} - m)$ at the bottom vertex, the first term is equal to zero (using the Dirac equation) times an integral which is not only linearly divergent on-mass-shell but also contains a parallel divergence, i.e., we find $(0/0)(a + b \ln(Q^2/m^2))$! It is standard practice (e.g., in proving the equivalence of different gauges) to drop this term, i.e., it is implicitly assumed that the theory is provided with an infrared cut-off which makes such ambiguous terms equal to zero on-mass-shell (e.g., by going to $4 + \epsilon$ dimensions, in which case $0/0 \to (p^2 - m^2)^{1+\epsilon}/(p^2 - m^2)$, or by giving the gluon a mass $\lambda$, in which case $0/0 \to (p^2 - m^2)/(p^2 - m^2 + \lambda^2)$). However, if we regulate the infrared divergences simply by going off-mass-shell, we will clearly obtain the "wrong" answer when we return to the mass-shell ($0/0 \to (p^2 - m^2)/(p^2 - m^2) = 1$). Presumably we would get the right answer for infrared-finite quantities (e.g., $\sigma(\gamma^* q \to q) + \sigma(\gamma^* q \to q + \text{soft gluon})$), in which the translation of $\not{k}$ to produce $\not{p} - m$ can introduce at most a logarithmic divergence, provided we treat real and virtual particles in the same way. Thus in gauges with $k_\mu k_\nu/(k^2)^2$ terms in the propagator we must either abandon our decision to consider only the production of transverse gluons and learn how to handle the discontinuity of $k_\mu k_\nu/(k^2)^2$ or stay on-shell (alternatively we may finesse the problem by interpreting $(p^2 - m^2)/(p^2 - m^2)$ as zero off-shell when we anticipate that such terms would vanish or cancel on -shell [13]). These problems occur also in the Feynman gauge in $O(g^4)$ and beyond when $k_\mu k_\nu$ terms are induced in the propagator by radiative corrections. They are avoided altogether in the stagnant Feynman gauge, in which these terms are absent diagram by diagram.

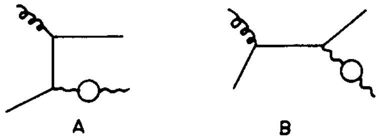

Fig. 9.

coefficient of the singularity is therefore proportional to figs. 1a,b evaluated with real physically polarized gluons.

Doing the $(\tilde{p} - \tilde{p}')$ phase space integral we find that the constant of proportionality is

$$\tfrac{2}{3}\lambda\, T_{\mathrm{F}} \ln(M^2/\tilde{p}^2)\,,$$

where $\tilde{p}^2 = \tilde{p}'^2$ is the mass of the produced quarks and $M^2$ is the invariant which controls the upper range of $\tilde{s}$: $t$ in the case of 8a and $s$ in 8b.

*CC3*: These contributions should be combined with the $q\bar{q}$ contribution to the wave-function renormalization of the produced gluon in fig. 1, indicated symbolically in fig. 9. Renormalization produces $\frac{2}{3}\lambda\, T_{\mathrm{F}} \ln(\tilde{p}^2/\mu^2)$, so the sum contains $\ln(M^2/\mu^2)$ only and is "mass finite" as $\tilde{p}^2 \to 0$ (KLN theorem). The net effect of $q\bar{q}$ radiation from the gluon line of fig. 1 is thus to modify it by the $q\bar{q}$ contribution to the renormalization factor $Z_3(M^2/\mu^2)$ *appropriate to a gluon propagating a distance $M^2$ from its mass-shell.* We shall see that radiation from outgoing lines always conspires to produce such an "effective" off-shell propagation factor.

Integrating over $t$ (or $s$), we obtain (we shall quote all results in units of $\lambda^2 W_n^0$):

$$W_n^{8\mathrm{a}+9\mathrm{a}} = \tfrac{1}{3} C_{\mathrm{F}} T_{\mathrm{F}} \left[\ln^2 \frac{Q^2}{\mu^2} - \ln^2 \frac{p^2}{\mu^2}\right] \int_0^1 \mathrm{d}y\, y^n \frac{1+y^2}{1-y}\,, \tag{3.1}$$

with the same contribution from 8b and 9b with $p^2 \to p'^2$ and $n = 0$ in the $y$ integral.

Next consider the two-gluon production diagrams of fig. 10. Simple kinematics establishes that in 10a and 10c:

*CC4*: $-t' > -t$, $s > s'$, so that the integrals over these variables are nested, e.g.,

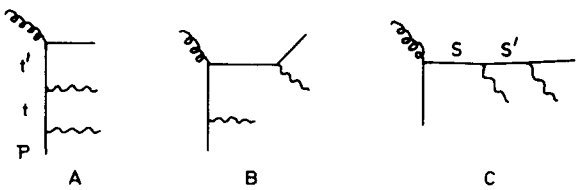

Fig. 10.

Table 1

Contributions of $O(g^4)$ diagrams, in units of $\lambda^2 W_n^0$. $C_F$, $C_G$, $T_F$, $r_n$, and $\upsilon$ are defined in the appendix, and $P \equiv \ln(Q^2/p^2)$, $P' \equiv \ln(Q^2/p'^2)$, $U \equiv \ln(Q^2/\mu^2)$, $R = \ln(p^2/\mu^2)$, $R' = \ln(p'^2/\mu^2)$

| Figure | Momentum configuration/ comment | Contribution to $W_n$ | Figure | Momentum configuration/ comment | Contribution to $W_n$ |
|---|---|---|---|---|---|
| 10a | | $\frac{1}{2}[C_F P r_n]^2$ | 8a+9a | | $\frac{1}{3}C_F T_F(U^2-R^2)r_n$ |
| 10b | | $[C_F P r_n][C_F P' r_0]$ | 8b+9b | | $\frac{1}{3}C_F T_F(U^2-R'^2)r_0$ |
| 10c | | $\frac{1}{2}[C_F P' r_0]^2$ | 11a+15a+15c | | $-\frac{5}{12}C_F C_G(U^2-R^2)r_n$ |
| 13g=13h | | $\frac{1}{2}[C_F P\upsilon][C_F P r_n]$ | 11b+15b+15d | | $-\frac{5}{12}C_F C_G(U^2-R'^2)r_0$ |
| 13i | | $[C_F P\upsilon][C_F P' r_0]$ | 17a | double UV | $\frac{5}{12}C_F C_G U^2$ |
| 13j=13k | | $\frac{1}{2}[C_F P'\upsilon][C_F P' r_0]$ | 17b | double UV | $-\frac{1}{3}C_F T_F U^2$ |
| 13l | | $[C_F P r_n][C_F P'\upsilon]$ | 17c=17g | double UV | $\frac{1}{4}(C_F^2-\frac{1}{2}C_F C_G)U^2$ |
| 12a | UV loop | $-\frac{1}{2}(C_F^2-\frac{1}{2}C_F C_G)(U^2-R^2)r_n$ | 17d=17h | double UV | $\frac{3}{4}(\frac{1}{2}C_F C_G)U^2$ |
| 12b | UV loop | $-\frac{3}{2}(\frac{1}{2}C_F C_G)(U^2-R^2)r_n$ | 17e=17f | double UV | $-\frac{1}{4}C_F^2 U^2$ |
| 12c | UV loop | $\frac{1}{2}(C_F^2)(U^2-R^2)r_n$ | 17i | double UV | $\frac{1}{4}C_F^2 U^2$ |
| 12d | UV loop | $-C_F^2 U P r_n$ | 17k | double UV | $\frac{1}{4}C_F^2 U^2$ |
| 12f | UV loop | $-\frac{1}{2}(C_F^2-\frac{1}{2}C_F C_G)(U^2-R'^2)r_0$ | | | |
| 12g | UV loop | $-\frac{3}{2}(\frac{1}{2}C_F C_G)(U^2-R'^2)r_0$ | | | |
| 12h | UV loop | $\frac{1}{2}(C_F^2)(U^2-R'^2)r_0$ | | | |
| 12i | UV loop | $-C_F^2 U P' r_0$ | | | |

Table 1 (continued)

| Figure | Momentum configuration/ comment | Contribution to $W_n$ | Figure | Momentum configuration/ comment | Contribution to $W_n$ |
|---|---|---|---|---|---|
| 17a | UV, $/\!/ p$ | $-\frac{5}{12}C_F C_G(U^2-R^2)v$ | 20a | $\equiv$ double $/\!/ p$ in fig. 17 *plus* $/\!/ p$ remainder | $\frac{1}{4}(C_F P v)^2$ |
| 17b | UV, $/\!/ p$ | $\frac{1}{3}C_F T_F(U^2-R^2)v$ | | | |
| 17c | UV, $/\!/ p$ | $-\frac{1}{4}(C_F^2-\frac{1}{2}C_F C_G)(U^2-R^2)v$ | | | |
| 17d | UV, $/\!/ p$ | $-\frac{3}{4}(\frac{1}{2}C_F C_G)(U^2-R^2)v$ | 20b | $\equiv(/\!/ p)(/\!/ p')$ in fig. 17 | $\frac{1}{2}(C_F P v)(C_F P' v)$ |
| 17e | UV, $/\!/ p$ | $\frac{1}{4}C_F^2(U^2-R^2)v$ | | | |
| 17f | UV, $/\!/ p$ | $-\frac{1}{4}(C_F^2-\frac{1}{2}C_F C_G)(U^2-R^2)v+$ "remainder" | 20c | $\equiv$ double $/\!/ p'$ in fig. 17 *plus* $/\!/ p'$ remainder | $\frac{1}{4}(C_F P' v)^2$ |
| 17g | UV, $/\!/ p$ | $-\frac{3}{4}(\frac{1}{2}C_F C_G)(U^2-R^2)v+$ "remainder" | | | |
| 17h | UV, $/\!/ p$ | $\frac{1}{4}C_F^2(U^2-R^2)v+$ "remainder" | | | |
| 17i | UV, $/\!/ p$ | $-\frac{1}{2}C_F^2 U P v$ | 20d | $\equiv$ double parallel logs in 17k | $\frac{1}{4}(C_F P v)^2+\frac{1}{2}(C_F P v)(C_F P' v)+\frac{1}{4}(C_F P' v)^2$ |
| 17k | UV, $/\!/ p$ | $-\frac{1}{2}C_F^2 U P v$ | | | |
| 17f | "remainder" | $-\frac{1}{2}(C_F^2-\frac{1}{2}C_F C_G)P^2 v$ | | | |
| 17g | "remainder" | $-\frac{3}{2}(\frac{1}{2}C_F C_G)P^2 v$ | | | |
| 17h | "remainder" | $\frac{1}{2}C_F^2 P^2 v$ | | | |
| 17a–h | UV, $/\!/ p'$ and "remainder" | same as UV, $/\!/ p$ with $R\to R'$, $P\to P'$ | | | |

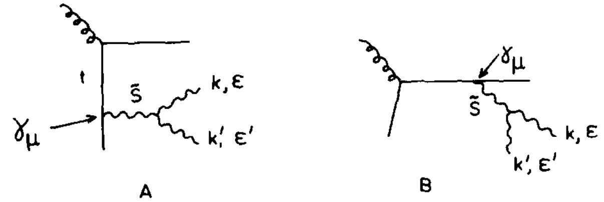

Fig. 11.

10a gives

$$\int_{p^2}^{Q^2} \frac{\mathrm{d}t'}{t'} \int_{p^2}^{t'} \frac{\mathrm{d}t}{t} = \tfrac{1}{2}\ln^2 \frac{Q^2}{p^2} \,. \tag{3.2}$$

This is the beginning of an exponential series $(1/n!)(\log)^n$ for such diagrams.

The resulting contributions of 10a and 10c are given explicitly in table 1.

Two gluons may also be produced through the gauge coupling in this order. This process (fig. 11) gives double logs when $\boldsymbol{k} \,/\!/\, \boldsymbol{k}'$ $((k+k')^2 \equiv \tilde{s} \simeq 0)$ and $\boldsymbol{k}+\boldsymbol{k}' \,/\!/\, \boldsymbol{p}$ or $\boldsymbol{p}'$ $(t \simeq 0$ or $s \simeq 0)$. The individual amplitudes behave as $\tilde{s}^{-1/2}$ times $t^{-1/2}$ or $s^{-1/2}$, so that each diagram contributes incoherently to leading logs (CC1). The $\gamma_\mu$ at the vertex indicated must couple to $\epsilon_\mu$, $\epsilon'_\mu$, $k_\mu$, or $k'_\mu$. Consider these factors in the double log configuration. Both $k_\mu$ and $k'_\mu$ are proportional to $p_\mu$ (or $p'_\mu$) and may therefore be dropped using the Dirac equation. Since $\boldsymbol{\varepsilon}$ and $\boldsymbol{\varepsilon}'$ are perpendicular to $\boldsymbol{k}+\boldsymbol{k}'$, it is clear that the contributions will be proportional to those of fig. 1 (CC2); integrating out the $k-k'$ phase space we find that the constant of proportionality is

$$C_{\mathrm{G}} \ln\frac{M^2}{k^2} \int_0^1 \mathrm{d}y \left[\frac{y}{1-y} + \frac{1-y}{y} + y(1-y)\right] , \tag{3.3}$$

where $k^2 = k'^2$ is the mass of the produced gluons, $k_\mu \simeq (y/(1-y))\, k'_\mu$ in the parallel configuration, and (as in the case of fig. 8) $M^2$ is $t$ or $s$. Shortly we shall find the contribution which renders the $y$-integral finite (CC5). Then (CC6) we shall see that the $k^2$ dependence is cancelled when we consider further $O(g^2)$ renormalizations of the gluon wave function.

Next we consider virtual radiative corrections to fig. 1 shown in fig. 12. First there are the *ultraviolet* $(|\boldsymbol{k}| \to \infty)$ logs due to the loops in all but 12e,j,k. These simply modify the $O(g^2)$ emission amplitudes by factors of $\ln(t/\mu^2)$ (12a–c), $\ln(s/\mu^2)$ (12f–h) or $\ln(Q^2/\mu^2)$ (12d,i). Integrating over $s$ or $t$ they give the contributions listed in the table.

These ultraviolet modifications are summed up in the shaded circles in figs. 13a–f; in this figure and *henceforth in similar diagrams*, shaded circles stand for *ultraviolet corrections only*.

The diagrams of fig. 12 also contribute to leading logs when the virtual gluons

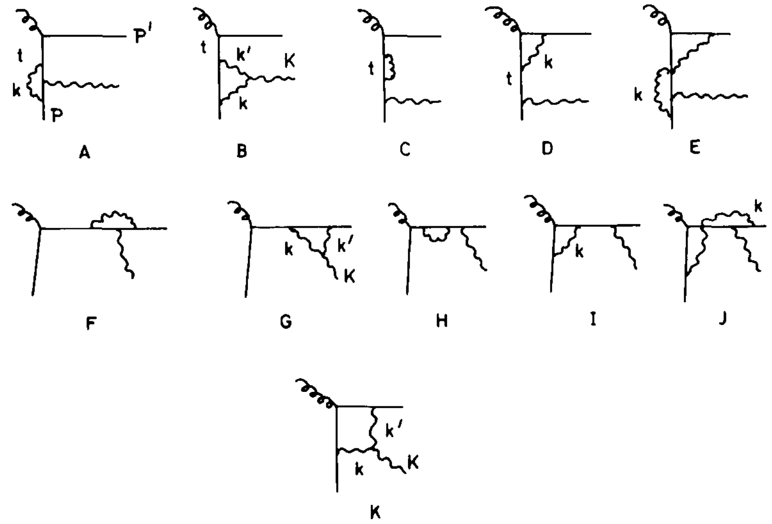

Fig. 12.

are near their mass-shells and emitted parallel to the quarks (real gluons are understood to be parallel to the line from which they are emitted). Let us consider diagrams 12a,b,d,e,i,j,k in the configuration $k^2 \simeq 0$, $k \parallel p$. (By the $p \leftrightarrow p'$ symmetry of fig. 12 it should be clear from this discussion how to compute the contribution of radiation parallel to $p'$.) In this configuration the virtual loop in 12d gives a $\ln(Q^2/t)$, to which we associate the effective diagram 13g (see fig. 7 for the notation used in fig. 13). We can evaluate this log and do the integral over $t$ immediately using (2.2) and (2.19) to obtain

$$W_n^{13g} = \tfrac{1}{2} C_F^2 \ln^2(Q^2/p^2) \langle r_n \rangle \langle v \rangle \, , \tag{3.4}$$

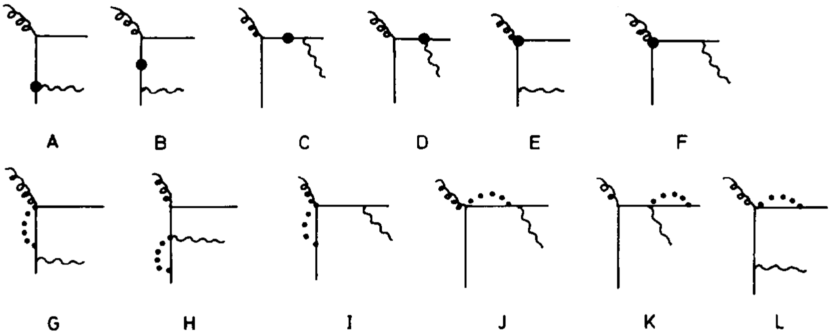

Fig. 13.

where

$$v \equiv \int_0^1 \mathrm{d}y \, \frac{-2y}{1-y}\,.$$

As in the case of fig. 4, the virtual logs in 12a,b,e,i,j,k arise when $k^2$ and $(p-k)^2$ are small and, since $k \,/\!/\, p$, we may write at the gluon vertex

$$\cdots (\not p - \not k)\,\gamma_\mu u(p) \simeq \cdots \frac{2y}{1-y}\, k_\mu u(p)\,. \qquad (3.5)$$

The contributions of these diagrams can then be combined using a Ward identity. We shall study these Ward identity manipulations in a more general way in sect. 4; in this order our results can easily be checked explicitly. As in familiar QED, the simplest QCD Ward identity states that $\partial_\mu A^\mu$ decouples from physical states (on-shell and transversely polarized in the case of gluons). Our procedure, applied to 12a,b,e,i,j,k, inserts a $\partial \cdot A$ (i.e., a gluon with $\epsilon_\mu \to k_\mu$) everywhere in the complete $O(g^2)$ amplitude for $\gamma^*$q → qg with only the initial quark unphysical. It is therefore no surprise that the Ward identity produces the amplitude for $\gamma^*$q → qg apart from a factor associated with the initial quark (as in the simpler case of fig. 4). The result can be expressed by figs. 13h,i, which the reader should now be able to evaluate.

Figs. 13j,k,l summarize the effects of virtual radiation parallel to $p'$.

We have not quite exhausted the parallel divergences due to virtual radiation in fig. 12. Figs. 12b,k,g are also logarithmic in the configuration $k^2, k'^2 \simeq 0$, $k \,/\!/\, k'$. Dropping terms which vanish in this configuration, the trigluon vertex is proportional to

$$(2k+k')_\alpha \epsilon_\beta - (2k'+k)_\beta \epsilon_\alpha \simeq \left(\frac{1+y}{1-y}\right) k'_\alpha \epsilon_\beta + \left(\frac{y-2}{y}\right) k_\beta \epsilon_\alpha$$

in the notation of fig. 14, where we have written $k_\mu \simeq (y/(1-y))\, k'_\mu$. The presence of the factors $k_\alpha$ and $k'_\beta$ means that once again $\partial \cdot A$ is involved and the amplitudes combine in a simple way due to Ward identities (we again defer further discussion; the result is easily checked explicitly in this order). The factor $\epsilon_{\alpha,\beta}$ ensures that the result is proportional to the amplitudes for $\gamma^*$q → qg. We represent it by the diagrams of figs. 15a,b, where the dotted line means that a factor

$$-\tfrac{1}{2} C_G \ln\frac{M^2}{k^2} \int_0^1 \mathrm{d}y \left(\frac{2-y}{y} + \frac{1+y}{1-y}\right) \frac{g^2}{8\pi^2}\,, \qquad (3.6)$$

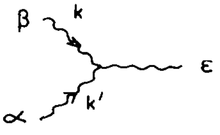

Fig. 14.

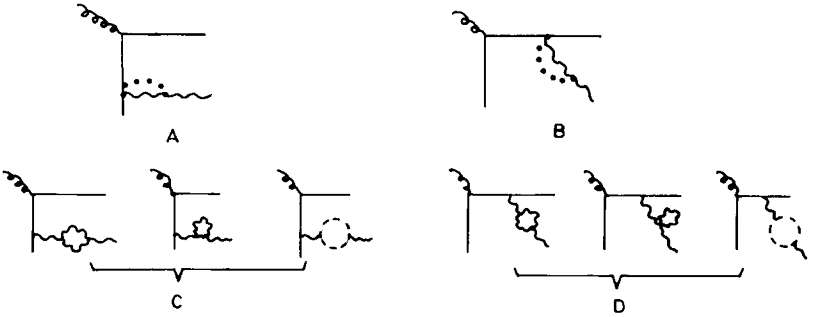

Fig. 15.

with $M^2 = t$, in 15a, $M^2 = s$ in 15b, multiplies the amplitude.

*CC5*: Combining figs. 15a,b (eq. (3.6)) and fig. 11 (eq. (3.3)) we get a $\gamma^* q \to qg$ term multiplied by the *infrared finite* factor:

$$\text{figs. } 11 + 15\text{a,b} \to -\tfrac{5}{6} C_G \ln(M^2/k^2)\,.$$

*CC6*: Combining this with the wave-function renormalizations symbolized in figs. 15c,d we get a result "mass finite" as $k^2 \to 0$:

$$\text{figs. } 11 + 15 \to -\tfrac{5}{6} C_G \ln(M^2/\mu^2)\,.$$

This factor amounts to the "renormalization" (given by $Z_3(M^2/\mu^2)$) *appropriate to a gluon propagating a distance $M^2$ from its mass-shell*, a feature we have already noted (CC3) for $q\bar{q}$ production.

*CC7*: The contributions of figs. 8a, 9a, 11a, 15a and 15c may be represented by fig. 16a, where the blob means multiply the bare diagram by the ultraviolet correction to a gluon propagating with invariant mass $t$. This is an element which will persist to all orders. (Figs. 8, 9, 11, 15b and 15d may be similarly represented.)

*CC8*: When fig. 16a and figs. 13a,b are taken together, the result is the same as what one would get by calculating fig. 1a with the *running coupling constant* $\bar{g}(t)$, where

$$\bar{g}^2(t) \simeq \frac{g^2}{1 + \frac{1}{2}\beta_0 g^2 \ln(t/\mu^2)} \simeq g^2 - \tfrac{1}{2}\lambda g^4 \left[\tfrac{11}{3} C_G - \tfrac{4}{3} T_F\right] \ln(t/\mu^2)\,. \qquad (3.7)$$

This combination is, of course, equal to the total contribution of the UV blobs in fig. 16b.

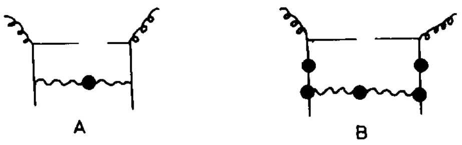

Fig. 16.

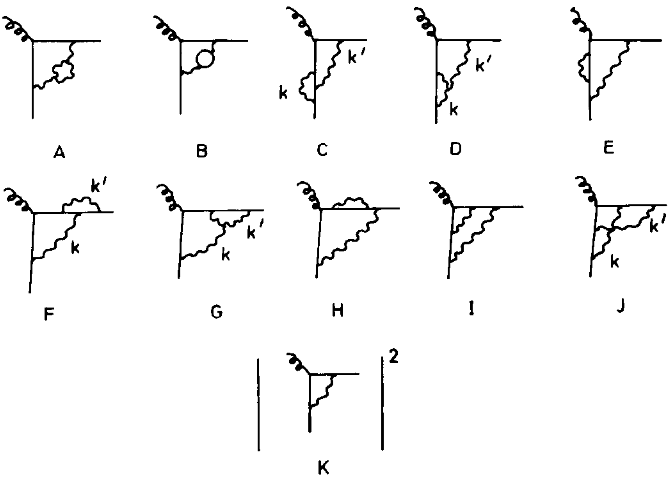

Fig. 17.

Finally we come to the $O(g^4)$ virtual corrections to elastic quark scattering (fig. 17). These diagrams contain double ultraviolet (UV) divergences, mixed UV and parallel divergences, and double parallel divergences. The "double UV" logs are easily evaluated using the renormalization group with the result shown in the table.

Next consider mixed parallel and UV logs. The UV logs due to superficially divergent subdiagrams are calculated first; we represent the consequent logarithmic modifications to the bare vertices and propagators by the blobs in fig. 18. The remaining parallel logs can now be evaluated as in the case of fig. 4 in sect. 2. Consider the $k /\!/ p$ region (the result for $k /\!/ p'$ is easily obtained with $p^2 \to p'^2$). In 18c the UV vertex gives $\ln(Q^2/\mu^2)$ and the result is just to multiply the $O(g^2)$ parallel log (eq. (2.19)) by the $O(g^2)$ UV log (2.14). In 18a,b,d the scale of the UV logs is $k_t^2/\mu^2$ (where $k_t$ was defined in eq. (2.7)). In 18e,f the scale is proportional to $k \cdot p'/\mu^2 \sim Q^2/\mu^2$. We shall write $\ln(Q^2/\mu^2) = \ln(k_t^2/\mu^2) + \ln(Q^2/k_t^2)$: the former log goes along with 18a,b and d; the latter "remainder" term will be combined with double parallel logs. The contribution to $W_n$ is obtained by logarithmic integration over $k_t^2$ and gives

$$W_n^{18a+b+d+e+f}(k /\!/ p) = -\tfrac{1}{4}C_F\left[\tfrac{11}{3}C_G - \tfrac{4}{3}T_F\right]\left(\ln^2\left(\frac{Q^2}{\mu^2}\right) - \ln^2\left(\frac{p^2}{\mu^2}\right)\right) v\,, \qquad (3.8)$$

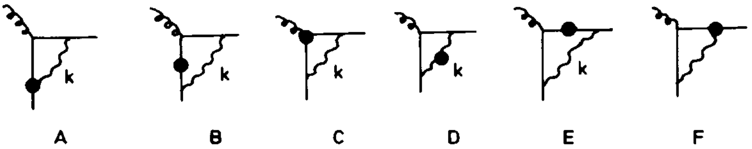

Fig. 18.

with "remainder"

$$W_n^{18\mathrm{e,f}}(\text{remainder}) = -\tfrac{1}{2} C_\mathrm{F} C_\mathrm{G} \ln^2(Q^2/p^2)\, v\,. \tag{3.9}$$

*CC9*: Eq. (3.8) is exactly the same as the term obtained by evaluating eq. (2.10) with $g^2$ replaced by the running coupling constant $\bar{g}^2(k_\mathrm{t}^2)$. In fact, we shall see that with $g \to \bar{g}$, eq. (2.10) gives the correct parallel log factor to all orders.

Last we consider "double parallel" logs from fig. 17 (17a,b,e and h do not contribute such terms), which we combine with "remainder" term (3.9) above. As with fig. 12, the various terms from fig. 17 can be combined using Ward identities. These identities will be discussed in sect. 4; in this order it is possible to verify the result explicitly, for which purpose it is convenient to proceed in two stages. First take $k /\!/ p$ or $k /\!/ p'$ in 17c,d,f,g,i,j. The result of summing insertions of the longitudinally polarized virtual gluons and combining the sum with "remainder" (3.9) is to produce terms which we represent in fig. 19 (the meaning of these figures should now be clear). The case in which the inner loop gives a UV log has already been discussed (fig. 18c). The result of extracting the parallel (both to $p$ and $p'$) logs from the inner loop is represented in figs. 20a–c (20d follows rather obviously from 17k). In figs. 20a and c the logarithmic integrals are rested (*cf.*, figs. 10a,c), e.g.,

$$\text{fig. 10a} \to \int_{p^2}^{Q^2} \frac{\mathrm{d}k_\mathrm{t}'^2}{k'^2} \int_{p^2}^{k_\mathrm{t}'^2} \frac{\mathrm{d}k_\mathrm{t}^2}{k_\mathrm{t}^2} = \frac{1}{2}\left(\ln \frac{Q^2}{p^2}\right)^2\,, \tag{3.10}$$

which again points to an exponential series.

It might appear that 20b emerges from these Ward identity manipulations twice – once from fig. 19a and once from fig. 19b – but this is illusory. The confusion is connected with a choice we have, in using Ward identity manipulations to isolate the $\ln(Q^2/p^2)\ln(Q^2/p'^2)$ contribution of fig. 17, whether to begin applying the identity first to gluons parallel to $p$ or to those parallel to $p'$. Of course the result must not depend on this choice – or our effective emission notation of fig. 20 fails! – and indeed it does not, but to see this in detail one must realize that only fig. 17j contributes $\ln(p^2)\ln(p'^2)$ (when $k /\!/ p$, $k' /\!/ p'$, *not* when $k /\!/ p'$, $k' /\!/ p$). The single diagram 20b represents this contribution. Fig. 20b is thus unambiguous and counts leading logs correctly. Verifying this statement (which corresponds to independence

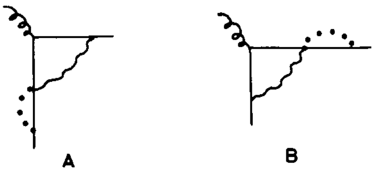

Fig. 19.

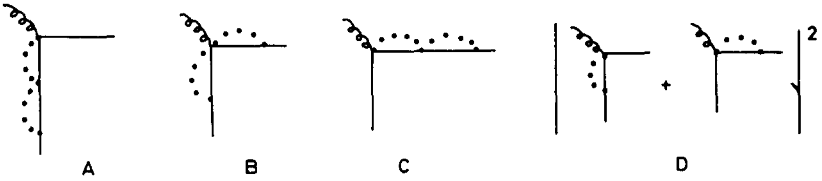

Fig. 20.

of the choice described above) in higher orders is elementary but lengthy, and we shall henceforth use notation like 20b freely *.

*CC10*: Combined with figs 18a,b,d,e, and f, fig. 20 gives the $O(g^4)$ term in the expansion of the exponential product

$$\exp\left[\lambda\, C_F\, v \int_{p^2}^{Q^2} \frac{dk_t^2}{k_t^2}\, \bar{g}^2(k_t^2)\right] \exp\left[\lambda\, C_F\, v \int_{p'^2}^{Q^2} \frac{dk_t^2}{k_t^2}\, \bar{g}^2(k_t^2)\right] . \tag{3.11}$$

These exponentials will play an important part in the final result; we shall denote multiplication by these exponentials by the notation of fig. 21; a hybrid of our effective virtual emission notation [indicating $v = \int_0^1 dy(-2y/(1-y))$] and our ultraviolet blobs (indicating $\bar{g}^2$).

We have now evaluated all the $O(g^4)$ contributions. It remains to assemble them all into a final result. First let us show that all singularities associated with $p'^2$ cancel, as they should from the KLN theorem. The double $p'^2$ logs are collected in fig. 22. They give the infrared-finite result

$$W_n^{22} = \frac{1}{2}\left[C_F(v+r_0)\ln\left(\frac{Q^2}{p'^2}\right)\right]^2 = \frac{1}{2}\left[\tfrac{1}{2}C_F \ln\left(\frac{Q^2}{p'^2}\right)\right]^2 .$$

Next evaluate fig. 23, where 23a is analogous to fig. 16b, and 23b (from which the remainder is dropped) contains 18a,b,d,e,f in the $\boldsymbol{k} /\!/ \boldsymbol{p}'$ configuration, giving

$$W_n^{23} = -\tfrac{1}{4}\left[\tfrac{11}{3}C_F - \tfrac{4}{3}C_G\right]\left[C_F(v+r_0)\right]\left[\ln^2\left(\frac{Q^2}{\mu^2}\right) - \ln^2\left(\frac{p'^2}{\mu^2}\right)\right]$$

$$= -\tfrac{1}{8}C_F\left[\tfrac{11}{3}C_F - \tfrac{4}{3}C_G\right]\left[\ln^2\left(\frac{Q^2}{\mu^2}\right) - \ln^2\left(\frac{p'^2}{\mu^2}\right)\right] .$$

Last, evaluate figs. 24a and b, corresponding to 13e and 18c (with $\boldsymbol{k} /\!/ \boldsymbol{p}'$) respec-

---

[*] The proof is a generalization of the statement, made above, that 17j does not contribute $\ln(p^2)\ln(p'^2)$ when $\boldsymbol{k} /\!/ \boldsymbol{p}'$, $\boldsymbol{k}' /\!/ \boldsymbol{p}$. The idea behind this is very simple: if momentum $\boldsymbol{k} /\!/ \boldsymbol{p}'$ enters the lower vertex in 17j, the fermion propagators are knocked "out of alignment" with $\boldsymbol{p}$, and we lose the $\ln(p^2)$. This argument also establishes, e.g., that 17i does not contribute $\ln(p^2)\ln(p'^2)$ in any momentum configuration.

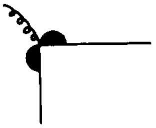

Fig. 21.

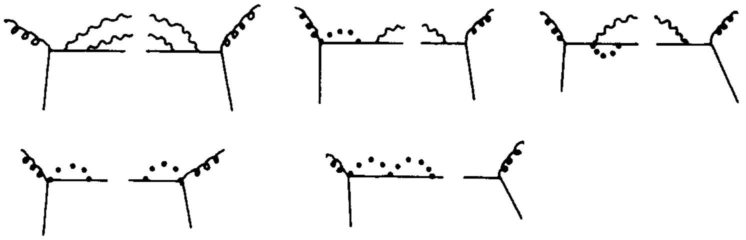

Fig. 22.

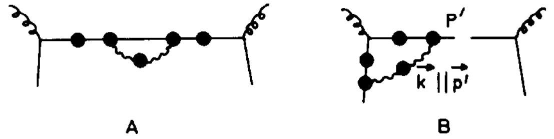

Fig. 23.

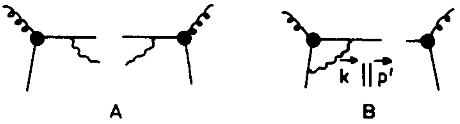

Fig. 24.

tively:

$$W_n^{24} = -\tfrac{1}{2} C_F^2 \ln\left(\frac{Q^2}{\mu^2}\right) \ln\left(\frac{Q^2}{p'^2}\right) .$$

The only other $p'^2$ logs in $W_n$ are provided by the renormalization factor $Z_3^F(p'^2/\mu^2)$:

$$Z_3^F\left(\frac{p'^2}{\mu^2}\right) = 1 + \tfrac{1}{2}\lambda\, C_F \ln\left(\frac{p'^2}{\mu^2}\right) + \tfrac{1}{8}\lambda^2\, C_F\, [C_F - (\tfrac{11}{3} C_G - \tfrac{4}{3} T_F)] \ln^2\left(\frac{p'^2}{\mu^2}\right) .$$

It is now a simple matter to verify that all the $p'^2$ singularities cancel in the final result. There remains a residuum of this cancellation in the form of a factor $Z_3^F(Q^2)$. Thus the effect of radiation from the $p'$ line is to provide a factor $Z_3^F(Q^2)$, just as corrections on the gluon lines produce $Z_3(t)$ (see CC6). This remarkable (though not

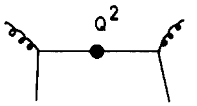

Fig. 25.

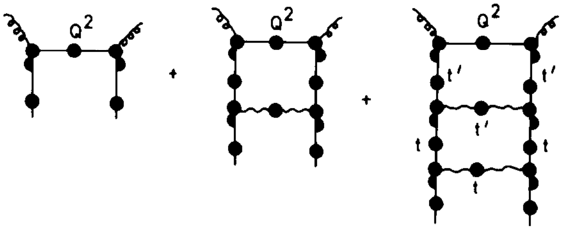

Fig. 26.

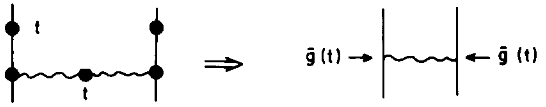

Fig. 27.

unexpected) result is represented by the blob in fig. 25.

*Final collection and comment*: We have now shown to $O(g^4)$ that the leading logs can be assembled into ladder structures as in fig. 26. Let us remind ourselves what the notation stands for and obtain the final result.

(i) The shaded circles represent *ultraviolet* renormalization factors only. Most of them combine conveniently to provide a running coupling constant at each rung, since (see fig. 27)

$$\frac{[Z_3^F(t)]^2\, Z_3(t)}{[Z_1^F(t)]^2} = \frac{\bar{g}^2(t)}{g^2}\,. \tag{3.12}$$

(ii) The shaded half-moons on the side-rails correspond to exponentials like (3.11). Taken together, they provide an overall factor $V$,

$$V(Q^2, p^2) = \exp\left[\lambda\, C_F\, v \int_{p^2}^{Q^2} \frac{dk_t^2}{k_t^2}\, \frac{\bar{g}^2(k_t^2)}{g^2}\right], \tag{3.13}$$

to $W_n$.

(iii) The remaining prescription is to evaluate fig. 28. The $t, t'$ integrals obviously lead to an exponential just like $V$, but containing $r_n$ instead of $v$. The corrections to the electromagnetic vertices satisfy a Ward identity which shows that each is equal to $[Z_3^F(Q^2/\mu^2)]^{-1}$. Thus one e.m. vertex correction cancels the blob on the top line and we are left with $[Z_3^F(Q^2/\mu^2)]^{-1}$ multiplied by $Z_3^F(p^2/\mu^2)$ from wave-function

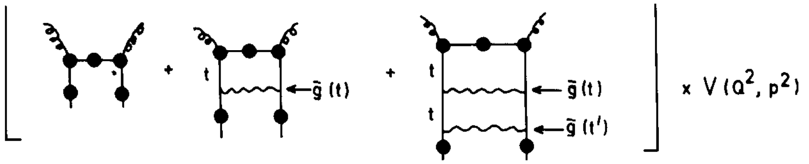

Fig. 28.

renormalization (indicated symbolically by blobs on the incoming lines). The final answer is

$$W_n = \exp\left[-\gamma_{n-1}^{\mathrm{NS}} \int_{p^2}^{Q^2} \frac{\mathrm{d}k_t^2}{k_t^2}\left(\frac{\bar{g}^2(k_t^2)}{g^2}\right)\right]$$

$$= \exp\left[-\gamma_{n-1}^{\mathrm{NS}} \int_{\mu^2}^{Q^2} \frac{\mathrm{d}x}{x}\left(\frac{\bar{g}^2(x)}{g^2}\right) + \gamma_{n-1}^{\mathrm{NS}} \int_{\mu^2}^{p^2} \frac{\mathrm{d}x}{x}\left(\frac{\bar{g}^2(x)}{g^2}\right)\right], \qquad (3.14)$$

which leads directly to eq. (1.3).

Eq. (3.14) is the correct answer, and fig. 28 (with up to infinitely many rungs) the correct prescription, to all orders, although at this point we have only checked it to fourth order. In subsequent sections we justify our prescription to all orders. We proceed explicitly, although we could have worked inductively if we had been prepared to assume infrared and KLN finiteness: in each order only a few new elements are introduced and finiteness is sufficient to determine them uniquely (it is easy to see that our results for parallel logs due to fig. 17 could have been derived in this way).

As far as we know, ours is the first explicit calculation of $W_n$ to $O(g^4)$. It can be used to deduce $\bar{g}^2(t)$ to $O(g^4)$ or, equivalently, the function $\beta(g)$ to $O(g^3)$. This is interesting since heretofore $\beta$ has been deduced from "unphysical" quantities. Writing

$$\bar{g}^2(t) = g^2 + A\,\frac{g^4}{16\pi^2}\ln\frac{t}{\mu^2} + \cdots,$$

various diagrams contribute to $A$ as follows:

$$\begin{aligned}
A(11\mathrm{a}+15\mathrm{a}+15\mathrm{c}) &= -\tfrac{5}{3}C_{\mathrm{G}}\,,\\
A(12\mathrm{a},\mathrm{UV}) &= C_{\mathrm{G}} - 2C_{\mathrm{F}}\,,\\
A(12\mathrm{b},\mathrm{UV}) &= -3C_{\mathrm{G}}\,,\\
A(12\mathrm{c}) &= 2C_{\mathrm{F}}\,,\\
A(8\mathrm{a}+9\mathrm{a}) &= \tfrac{4}{3}T_{\mathrm{F}}\,,\\
A(\mathrm{total}) &= -\tfrac{11}{3}C_{\mathrm{G}} + \tfrac{4}{3}T_{\mathrm{F}}\,.
\end{aligned}$$

Note that:

(i) The contributions proportional to $C_F$ are the same as in the abelian case and cancel due to the abelian Ward identity $Z_1 = Z_2$.

(ii) The screening contribution proportional to $T_F$, due to $q\bar{q}$ production, is also essentially the same as in the abelian case (where it gives the total contribution).

(iii) The remaining contributions are essentially non-abelian in character, being proportional to $C_G$. The negative (antiscreening) part is due entirely to diagrams involving the trigluon coupling: the ultraviolet contribution of fig. 12b and the parallel logs of 12b and 12k combined in 15A (we regard the role of wave-function renormalization, 15c, as being merely to change the scale of 11a + 15c from $k^2$ to $\mu^2$). We can, if we wish, interpret the decrease of $\bar{g}^2(t)$ caused by these diagrams as being due to a "spreading out" of the fermion colour charge seen by the bifurcated gluon.

## 4. Parallel logs and Ward identities

In this section we derive the parallel log factor (eq. (3.13)) and obtain the corresponding factor for the case of external gluons, which is needed in the mixing section. We consider explicitly the factors associated with incoming particles; the factors for outgoing particles are obviously the same.

Consider fig. 29, where here and below the symbol ⊓ means that the amplitude is one particle irreducible in the channel composed of the particles it brackets (the incident quark channel in this case). Otherwise the amplitude is complete, i.e., it contains all corrections to the other external lines. Apart from the incident quark and virtual photon, all the other external particles are physical – on-shell and transversely polarized in the case of gluons.

We proceed up the incident gluon line until we encounter the first "parallel" gluon which we exhibit in fig. 30a. Note that this must be associated with a $k /\!/ p$ log: if $k$ were parallel to an outgoing line $p + k$ would not be parallel to $p$ and we would lose a log. Dropping terms which do not produce singularities as $p^2 \to 0$, we can replace the factor $(\not{p} - \not{k})\,\gamma_\mu$ from the quark propagator and vertex by $2(y/(1-y))\,k_\mu$, as in eq. (2.9). The factor $k_\mu$ allows us to use Ward identities. Since these relate complete amplitudes it is convenient to replace fig. 30a by 30b.

The relevant identity is shown in fig. 31, where the dashed line is a Faddeev-Popov ghost field $(\phi^a)$, $a$ and $i$ are colour indices, $J_0^a$ and $J_1^i$ are sources and $\alpha$ is the gauge-fixing parameter (or gauge-fixing function $\alpha(k^2)$ in our case). When the ghost

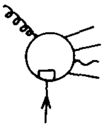

Fig. 29.

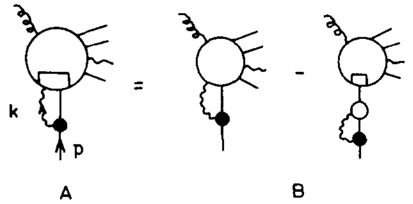

Fig. 30.

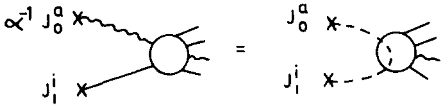

Fig. 31.

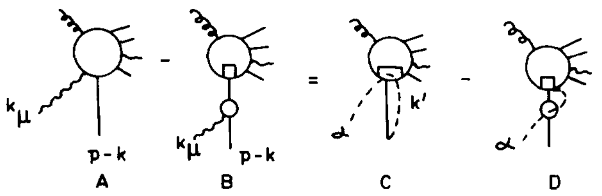

Fig. 32.

passes through the blob it can interact in all possible ways (note that the sources of the other particles could also serve as ghost "sinks" if they were not physical). The interactions with the sources are $J_0^a \partial^\mu A_\mu^a$ and $\psi^i J_1^i$ on the left (suppressing spinor indices) and $J_0^a \phi^a$ and $g\phi^a \psi_i \frac{1}{2}\lambda_{ij}^a J_1^i$ on the right. This is a special case of the Slavnov-Taylor-Ward identities derived by 't Hooft and Veltman [14]. It expresses directly the invariance of $\langle 0 | T(\phi^* AA \ldots A\psi \ldots \psi) | 0\rangle$ under Becchi-Rouet-Stora (BRS) transformations [15].

Using fig. 31 we can rewrite part of 30b in the way shown in fig. 32 (there are other terms, generated by both 32a and b, in which the ghost couples to the incident quark source but they cancel). The first term (fig. 32c) on the right does not contribute to singularities as $p^2 \to 0$ and can be dropped in LLA. We denote its contribution by

$$\int \frac{d^4k'}{k^2 k'^2} M \frac{1}{\not{p} - \not{k} - \not{k}'} .$$

On the left we have

$$\frac{1}{k^2} k^\mu M_\mu \frac{1}{\not{p} - \not{k}} ,$$

where $M_\mu$ represents the total (one particle irreducible) contribution of the upper parts of 32a and b. However, we have used $(\not{p} - \not{k})\gamma_\mu$ to generate $k_\mu$ so we actually need

$$\frac{1}{k^2} k^\mu M_\mu \frac{1}{(p-k)^2} = \int \frac{\mathrm{d}^4k'}{k^2 k'^2 (p-k)^2} M \frac{1}{(\not{p} - \not{k} - \not{k}')} (\not{p} - \not{k}) + (\text{32d term}) \, .$$

The 32c term can therefore be dropped in leading log approximation since $(\not{p} - \not{k}) \propto p$ in the parallel configuration and $\not{p}$ kills the potential log from the $p$ line if it is virtual (or gives $\not{p}u\,(p) \to 0$ if it is real).

Thus only 32d survives. In this diagram the ghost quark interaction involves only the single scale $(p-k)^2 \simeq k^2 = k_\mathrm{t}^2$. Therefore, it only contains UV logs (with argument $k_\mathrm{t}^2/\mu^2$) and we may redraw the bottom half of 32d as shown in fig. 33. Finally, the parallel log due to 30a may be represented by fig. 34 where the diagram on the left has the meaning discussed earlier (fig. 7) and the blob on the right represents the function of $k_\mathrm{t}^2/\mu^2$ due to $\alpha(k^2) \times$ all UV logs. We now collect and analyse the latter factors which are:

(i) $\alpha(k^2)$, introduced by the Ward identity; this is just the contribution of the correction to the bare gluon propagator (see eq. (1.4)) in fig. 30a;

(ii) The corrections to: (a) the quark gluon vertex in fig. 30a, (b) the quark propagator in fig. 33, (c) the ghost propagator in fig. 33, (d) the ghost quark Ward identity vertex in fig. 33.

The factors (iia) and (iib) above combine with $\sqrt{\alpha}(k^2)$ to turn one factor of $g$ into $\bar{g}(k_\mathrm{t}^2)$ in the lowest-order prescription for the parallel log factor. The behaviour of the remaining factors is determined by their anomalous dimensions, which are obtained from the factors which renormalize them. These are: $Z_3^{-1/2}$ for $\sqrt{\alpha}(k^2)$, $\tilde{Z}_3^{-1}$ for factor (iic) and $\tilde{Z}_1 Z_3^{3/2}/Z_1$ for factor (iid) (this follows from the fact that $g_0$ is renormalized by $Z_3^{3/2}/Z_1$ and, as shown by Brandt [15], $\tilde{Z}_1 \lambda_{ij}^a \phi^a \psi_j$ is a finite operator if $\phi$ and $\psi$ are renormalized fields). The product of these factors is

$$\frac{\tilde{Z}_1 Z_3}{\tilde{Z}_3 Z_1} ,$$

which is just one by the Slavnov-Taylor identity [17]. The net effect is, therefore, that the other factor of $g$ in the lowest-order parallel log factor should also be replaced by $\bar{g}(k_\mathrm{t}^2)$.

We can now proceed up the incident line in fig. 34 treating subsequent parallel

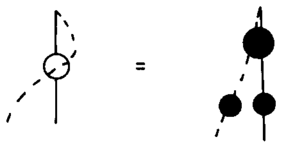

Fig. 33.

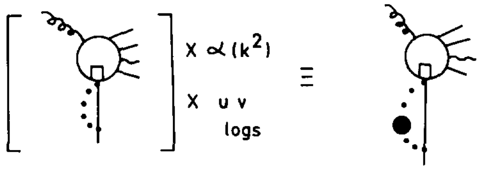

Fig. 34.

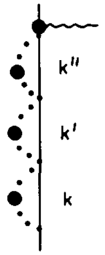

Fig. 35.

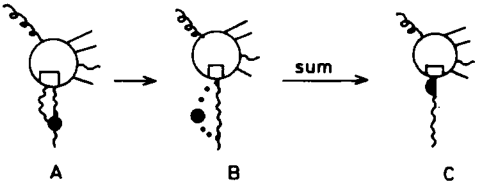

Fig. 36.

gluons in the same way. The limits of the $k_t^2$ integrals are determined by the neighbouring invariants, which set the scale of deviations from the simple $(k_t^2)^{-1}$ factors in the integrands. Thus, for example, corresponding to fig. 35 we obtain

$$\int_{p^2}^{t} \bar{g}^2(k_t''^2)\frac{\mathrm{d}k_t''^2}{k_t''^2}\int_{p^2}^{k_t''^2} \bar{g}^2(k_t'^2)\frac{\mathrm{d}k_t'^2}{k_t'^2}\int_{p^2}^{k_t'^2} \bar{g}^2(k_t^2)\frac{\mathrm{d}k_t^2}{k_t^2}$$

in leading log approximation. Finally summing all the parallel factors we obtain the exponential factor $V$ of eq. (3.13).

It is worth remarking that this technique can be used to sum leading logs which are contributed by crossed ladders in the case that we choose to perform covariant spin sums for produced gluons (which means that we must also include ghost production). This leads to effective ladder diagrams (as discussed by Gribov and Lipatov [3] in the much simpler abelian case).

We also need parallel log factors associated with external gluons as illustrated in fig. 36 (we already encountered such logs in (3.6)). The argument presented for the quark case goes through with only minor modifications. The result is that with $g^2 \to \bar{g}^2(k_t^2)$ eq. (3.6) describes the factor in fig. 36b and summation produces the factor represented in fig. 36c:

$$\exp\left[-\tfrac{1}{2}\lambda\, C_G \int_0^1 dy\left(\frac{2-y}{y}+\frac{1+y}{1-y}\right)\int \frac{dk_t^2}{k_t^2}\left(\frac{\bar{g}^2(k_t^2)}{g^2}\right)\right]. \tag{4.1}$$

## 5. The complete non-singlet result to leading order in $\bar{g}^2$

We have now established to all orders all the elements of the prescription for calculating leading logs presented at the end of sect. 3. The related prescription for calculating "fragmentation functions" in LLA can be obtained by the same arguments; it is illustrated in fig. 37 where we have opened up the blob on the top rung of a ladder to obtain a rainbow.

This leading log prescription cannot be used directly to obtain realistic results since the leading log expansion of $\bar{g}^2(t) \sim 1/\ln t$ is only adequate for large $t$ and the invariants in our diagrams have lower limits of order $p^2$. The cure involves the introduction of another scale $M$, large enough that we are prepared to neglect $\bar{g}^2(M^2)$ compared to 1, which is used to separate parts of the diagram carrying momenta smaller and larger than $M$ (this procedure is the diagrammatic realisation of eq. (1.2)).

Our prescription is useful wherever the invariants are large and implies that only ladders can sustain large momenta ($t$) to leading order in $\bar{g}^2(t)$. Therefore to leading order in $\bar{g}^2(Q^2)$ every diagram begins as a ladder, as shown in fig. 38 line 1 (where we omit UV blobs and parallel log correction factors for simplicity). We can split the $t$-integral into the regions $|t| \geqslant M^2$ and $|t| < M^2$, as indicated in line 2. For $|t| < M^2$ we can say nothing since $t$ runs down to $O(p^2)$. Accordingly we draw a "black box", representing an unknown function $N(x, t)$ ($N$ for non-singlet) which gives the probability of finding a quark with "mass" equal to $t$ ($|t| < M^2$) and momentum fraction $x$. For $|t| \geqslant M^2$ large momentum enters the next vertex which must therefore have a ladder structure to leading order in $\bar{g}^2(M^2)$. Proceeding to split up the $t'$ and subsequent integrals in the same way we arrive at the last line of fig. 38.

We now write the parallel log factor (see (3.13)) at the bottom rung as $V(t_n, t) =$

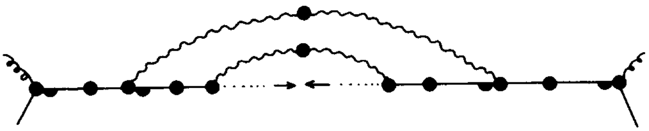

Fig. 37.

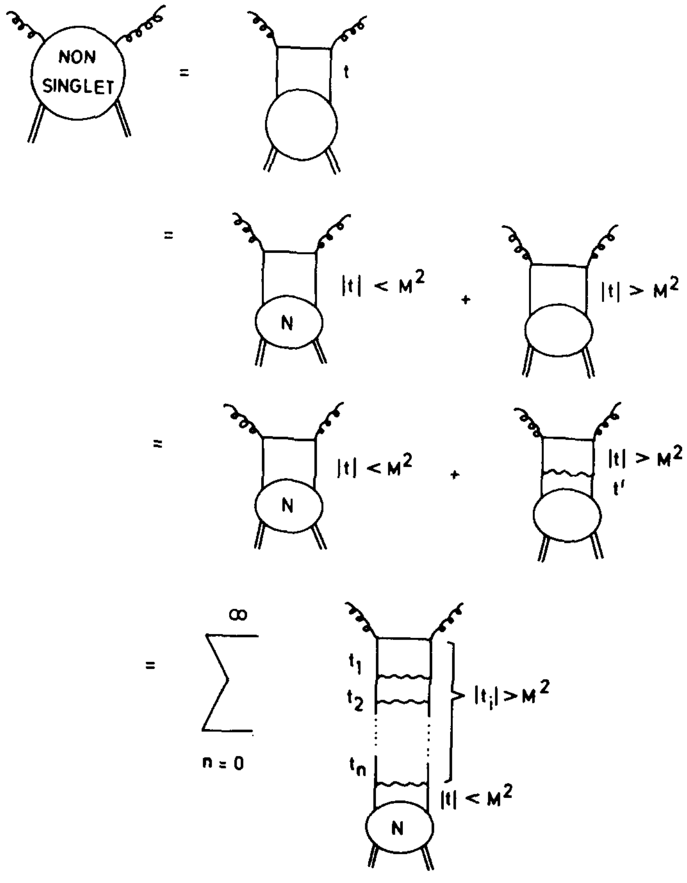

Fig. 38.

$V(t_n, M^2)\, V(M^2, t)$ and associate the second factor with the black box. Integrating over $t$ and taking moments, our ignorance of the hadron vertex is isolated in

$$N_n(M^2) = \int_0^1 x^{n+1}\, \mathrm{d}x \int_{p^2}^{M^2} \frac{\mathrm{d}t}{t} V(M^2, t)\, N(x, t)\,.$$

For $M^2 = Q^2 = |t|_{\max}$ only the first term in line 2 survives and we see that $N_n(M^2) = W_n(M^2)$. For $Q^2 \geqslant M^2$ this is modified by the ladder sum for scattering on a quark of "mass" $M$:

$$[Z_3^{\mathrm{F}}(Q^2)]^{-1} \left\{ \sum_{m=0}^{\infty} (\lambda\, C_{\mathrm{F}} r_n)^m \int_{M^2}^{Q^2} \frac{\mathrm{d}t_1}{t_1} \bar{g}^2(t_1) \cdots \int_{M^2}^{t_{m-1}} \frac{\mathrm{d}t_m}{t_m} \bar{g}^2(t_m) \right\}$$

$$\times \exp\left[\lambda\, C_{\mathrm{F}}\, v \int_{M^2}^{Q^2} \frac{\mathrm{d}x}{x}\, \bar{g}^2(x)\right] = \left\{\frac{\bar{g}^2(Q^2)}{\bar{g}^2(M^2)}\right\}^{2\gamma_{n-1}^{\mathrm{NS}}/g^2\beta_0} ,$$

where the provenance of each factor should by now be clear. The factorization of the ladder sum into a function of $Q^2$ and a function of $M^2$ ensures that the result is independent of the choice of the large scale $M$, which is necessary for consistency. The final result is, of course, eq. (1.3).

## 6. Singlet structure functions and mixing

The singlet structure function, like the non-singlet, is computed by exposing ladders wherever large momentum transfer flows, as in fig. 39. There are now two possibilities for the black box: the hadron vertex can deliver up a gluon or a (singlet) quark. The relative probabilities for these two processes to occur is absorbed into (incalculable) factors $G_n(M^2)$ and $S_n(M^2)$, respectively, analogous to $N_n(M^2)$ in sect. 5. Our task is to evaluate the $Q^2$ behaviour of the ladder sums. (The blobs at the e.m. vertex and on the top rung combine to give a factor $[Z_3^{\mathrm{F}}(Q^2)]^{-1}$, as before.)

The only new feature in the singlet case is the possibility of having gluon siderails in the ladder, leading to new rung elements shown in fig. 40. Fig. 40a is already familiar to us: the q → qg skeleton gives a factor $\lambda C_{\mathrm{F}} r_n$, the blobs combine (using (3.12)) to give $\bar{g}^2(t)$, and the half-moons signify the virtual radiation factor (3.13):

$$A_n \sim \lambda\, C_{\mathrm{F}} r_n \frac{\mathrm{d}t}{t}\, \bar{g}^2(t) \exp\left[\lambda\, C_{\mathrm{F}}\, v \int^{t} \frac{\mathrm{d}x}{x}\, \bar{g}^2(x)\right] .$$

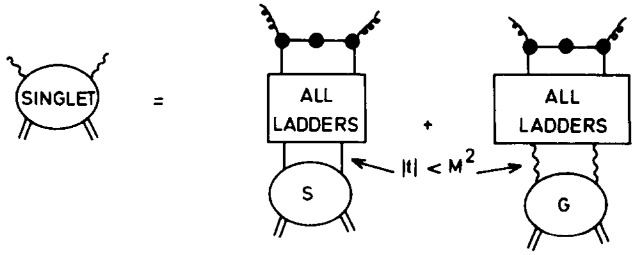

Fig. 39.

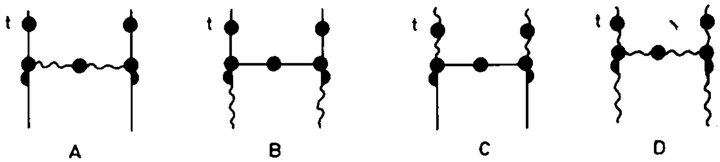

Fig. 40.

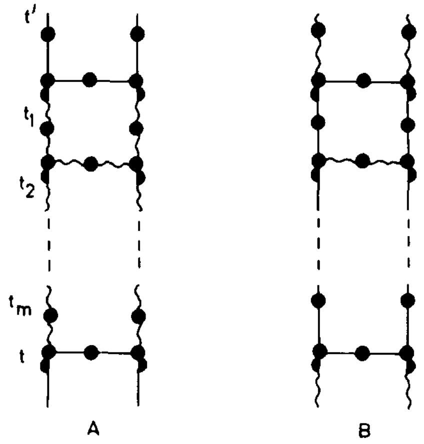

Fig. 41.

The (infrared-finite) skeleton factors associated with 40b,c are easily calculated (see the appendix). The blobs in these elements do not quite combine to give $\bar{g}^2(t)$, the difference being ratios of $Z$ factors:

$$B_n \sim -\gamma_{n-1}^{\mathrm{QG}} \frac{\mathrm{d}t}{t} \bar{g}^2(t) \frac{Z_3^{\mathrm{F}}(t)}{Z_3(t)} \exp\left[\lambda\, C_{\mathrm{F}}\, \nu \int^{t} \frac{\mathrm{d}x}{x} \bar{g}^2(x)\right] ,$$

$$C_n \sim -\gamma_{n-1}^{\mathrm{GQ}} \frac{\mathrm{d}t}{t} \bar{g}^2(t) \frac{Z_3(t)}{Z_3^{\mathrm{F}}(t)} \exp\left[\lambda\, C_{\mathrm{F}}\, \nu \int^{t} \frac{\mathrm{d}x}{x} \bar{g}^2(x)\right] .$$

The (infrared-divergent) skeleton factor for 40d is obtained from (3.3) by inserting $y^n$, giving a factor $\rho_n$ defined in the appendix:

$$D_n \sim \lambda\, C_{\mathrm{G}}\, \rho_n \frac{\mathrm{d}t}{t} \bar{g}^2(t) \exp\left[\lambda\, C_{\mathrm{F}}\, \nu \int^{t} \frac{\mathrm{d}x}{x} \bar{g}^2(x)\right] .$$

At first sight it seems that the factors of $Z_3$ and $Z_3^{\mathrm{F}}$ in 40b,c might prevent us obtaining the expected prescription. However, these factors combine in a simple way when we connect 40b and 40c with pure gluon ladders constructed from 40d. The portion of a ladder shown in fig. 41a contributes:

$$\text{fig. 41a} \sim \left[-\gamma_{n-1}^{\mathrm{QG}}\, \bar{g}^2(t') \frac{\mathrm{d}t'}{t'} \frac{Z_3^{\mathrm{F}}(t')}{Z_3(t')}\right] \left[-\gamma_{n-1}^{\mathrm{GQ}}\, \bar{g}^2(t) \frac{\mathrm{d}t}{t} \frac{Z_3(t)}{Z_3^{\mathrm{F}}(t)}\right]$$

$$\times \left\{\sum_m (\lambda\, C_{\mathrm{F}}\, \rho_n)^m \int_t^{t'} \frac{\mathrm{d}t_1}{t_1} \bar{g}^2(t_1) \cdots \int_t^{t_{m-1}} \frac{\mathrm{d}t_m}{t_m} \bar{g}^2(t_m)\right\}$$

$$\times \exp\left[\lambda\, C_{\mathrm{G}}\,\nu \int_{t_1}^{t'} \frac{\mathrm{d}x}{x}\,\bar{g}^2(x)\right] \cdots \exp\left[\lambda\, C_{\mathrm{G}}\,\nu \int_{t}^{t_m} \frac{\mathrm{d}x}{x}\,\bar{g}^2(x)\right] \tag{6.1}$$

$$= \left[-\gamma^{\mathrm{QG}}_{n-1}\,\bar{g}^2(t')\,\frac{\mathrm{d}t'}{t'}\right] \exp\left[-(\gamma^{\mathrm{GG}}_{n-1} + 2\gamma_{\mathrm{F}}) \int_t^{t'} \frac{\mathrm{d}x}{x}\,\bar{g}^2(x)\right] \left[-\gamma^{\mathrm{GQ}}_{n-1}\,\bar{g}^2(t)\,\frac{\mathrm{d}t}{t}\right],$$

where we have expressed $(\rho_n + \nu)$, $Z_3$, and $Z_3^{\mathrm{F}}$ in terms of $\gamma_{\mathrm{A}}$ and $\gamma_{\mathrm{F}}$, using the formulas in the appendix. Likewise, 40c and 40b are connected by pure quark ladders constructed from 40a, giving for fig. 41b:

$$\text{fig. 41b} \sim \left[-\gamma^{\mathrm{GQ}}_{n-1}\,\bar{g}^2(t')\,\frac{\mathrm{d}t'}{t'}\right]$$

$$\times \exp\left[-(\gamma^{\mathrm{NS}}_{n-1} + 2\gamma_{\mathrm{F}}) \int_t^{t'} \frac{\mathrm{d}x}{x}\,\bar{g}^2(x)\right] \left[-\gamma^{\mathrm{GQ}}_{n-1}\,\bar{g}^2(t)\,\frac{\mathrm{d}t}{t}\right]. \tag{6.2}$$

It follows from (6.1), (6.2) that, if we intend to perform the ladder sums, we can associate with the vertices the effective matrix factor

$$\begin{pmatrix} A & B \\ C & D \end{pmatrix}_n \sim [\Gamma_n - 2\gamma_{\mathrm{F}} I]\,\frac{\mathrm{d}t}{t}\,\bar{g}^2(t)\,, \tag{6.3}$$

where $\Gamma_n$ is the anomalous dimension matrix defined in the appendix and $I$ the unit matrix. The elements of matrix $(\Gamma_n - 2\gamma_{\mathrm{F}} I)^m$ give the factors associated with all $m$-rung ladders (with incoming and outgoing quark or gluon lines) which can be constructed out of figs. 40a–d. The $Q^2$ dependence of the ladder sum of fig. 39 is then given by the eigenvalues $d^{\pm} - 2\gamma_{\mathrm{F}}$ of the matrix $\Gamma - 2\gamma_{\mathrm{F}} I$ ($d^{\pm}$ are the eigenvalues of $\Gamma$). The extra dependence involving $2\gamma_{\mathrm{F}}$ is removed by the blobs on the top rung, giving the final result that $\widetilde{W}_n$ is a linear combination of two terms with $Q^2$ dependences $[\bar{g}^2(Q^2)]^{2d^{\pm}/g^2\beta_0}$.

## 7. Concluding remarks

Our methods provide explicit verification of factorization, etc., in LLA and allow us to derive the ladder structure, which is the basis of the parton model (and the Kogut-Susskind [18], Altarelli-Parisi [12] interpretation of the RGE), using elementary techniques – much of the physics being apparent in $O(g^2)$. Beyond the leading log approximation the virtues of our approach decrease rapidly. It can be used to demonstrate factorization to all orders but the terminology and machinery needed become increasingly cumbersome and this is not compensated by the ability to calculate explicitly or by new insights. All-orders proofs seem simplest in the axial gauge (although here also the identification of hard scattering kernels, anomalous dimension, etc., with diagrammatic structures is complex beyond leading order and does not offer much insight).

Information about jet structure, multi-jet cross sections, etc., in deep inelastic scattering is easily obtained using our methods. For example, it is clear that the dominant contribution consists of two jets and that there is a subdominant O($\alpha_s$) three jet structure, with a cross section given by the prescription of Ellis et al. [19] and Floratos [20] (this is shown explicitly in ref. [13] where earlier arguments [21] are extended to the non-abelian case).

Our techniques have many other applications. For example, they can be used to rederive and interpret predictions for deep inelastic scattering on a photon [22], which were originally derived using the OPE. Furthermore it should be clear that they apply to other hard processes as well as deep inelastic scattering (e.g., to the production of heavy $\mu$-pairs).

As an example we consider the production of heavy quarks (Q) in pp collisions, where the proper use of QCD perturbation theory is especially easy to understand using the diagrammatic approach. Many phenomenologists have assumed that fig. 42 gives the dominant contributions, where the open circles represent the momentum-dependent quark or gluon distributions and the subprocesses is evaluated using $\bar{g}$ at some author dependent scale. This is correct in LLA in the (impossible!) limit $s \to \infty$ with $M_Q^2/s$ fixed (typical choices of $\bar{g}$ only differ in the next to leading terms); in this limit

$$-\hat{t}_{\min} = -M_Q^2 + \tfrac{1}{2}\hat{s}\left(1 - \sqrt{1 - \frac{4M_Q^2}{s}}\right) \to \infty\,, \qquad \hat{s} \geqslant 4M_Q^2 \to \infty\,,$$

so the large $\hat{t}\,[\hat{s}]$ in 42a[42b,c] arranges the rest of the diagram into ladders, as in deep inelastic scattering [heavy $\mu$-pair production]. As $s \to \infty$ with $M_Q^2$ fixed, however, it is clear that QCD perturbation theory will become useless since $-\hat{t}_{\min} \to 0$. The picture is only useful, therefore, for $M_Q^2$ large and $\hat{s}$ "not too far from threshold" (in practice $\langle \hat{s} \rangle$ may remain of order $4M_Q^2$ up to quite large $s$ due to the steepness of the quark and gluon distributions).

Quantitatively we obtain precise predictions for the moments of the cross section corresponding to fig. 42. These momenta factorize and the predictions have the

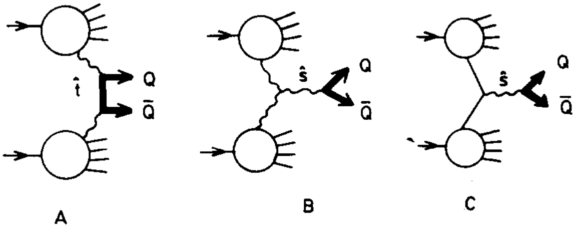

Fig. 42.

(symbolic) parton model interpretation

$$\int_1^\infty \sigma(s, M_Q^2)\frac{dz}{z^n} = \int_0^1 x^{n-1} q(x, M_Q^2)\, dx \int_0^1 x'^{n-1} q'(x', M_Q^2)\, dx$$

$$\times \int_1^\infty \hat{\sigma}(\hat{s}, M_Q^2)\frac{d\hat{z}}{\hat{z}^n} ,$$

where $z = s/4M_Q^2$, $\hat{z} = \hat{s}/4M_Q^2$. The integrals only converge for $n \geqslant 2$ (or $n \geqslant 1$ in the non-singlet case), so these precise predictions are indeed only sensitive to $s$ near threshold, as anticipated and interpreted above.

This is just one example of the utility of the diagrammatic interpretation of hard scattering processes.

We are grateful to John Taylor for numerous useful discussions. One of us (A.B.C.) thanks the Rhodes trust for the award of a Rhodes Scholarship and the other thanks the S.R.C. for support.

## Appendix

In this appendix we compile the notations and conventions used throughout this paper. Rules for Feynman diagrams are those found in ref. [23], with the exception that our spinors are normalized so that $\bar{u}u = 2m$. We use the standard convention that $Q^2 = -q^2 = \boldsymbol{q}^2 - q_0^2 \geqslant 0$ in deep inelastic scattering. The effective expansion parameter is

$$\lambda \equiv \frac{g^2}{8\pi^2} .$$

### *A.1. Figures*

In figures a wavy line (∿∿∿) is a gluon, a dashed line (– – –) a ghost, a solid line (———) a quark, the inductance symbol (ℓℓℓℓℓ) a virtual photon, and a dotted line (· · · · ·) indicates the effective contribution (summed up with Ward identities) of virtual parallel radiation.

### *A.2. Lie group factors*

$C_F$ = quadratic Casimir eigenvalue for fundamental (quark) representation,

$$= \frac{1}{2N}(N^2 - 1) \text{ for SU}(N) ,$$

$C_G$ = quadratic Casimir eigenvalue for adjoint (gluon) representation

$= N$ for SU($N$) ,

$T_F = \frac{1}{2}$(number of flavours).

### *A.3. The renormalization group and anomalous dimensions*

The normalization of our anomalous dimensions and $\beta$-function is fixed relative to renormalization group equation (written here symbolically; $G$ is some function with definite renormalization group transformation properties):

$$\left[\frac{\partial}{\partial \ln \mu^2} + \beta \frac{\partial}{\partial g} - \gamma\right] G = 0 \,. \tag{A.1}$$

This normalization may differ (by factors of two) from those used by other authors. Here

$$\beta(g) = -\tfrac{1}{4}\beta_0 g^3 + O(g^5) \,,$$

with

$$\beta_0 = \frac{1}{8\pi^2} \left[\tfrac{11}{3} C_G - \tfrac{4}{3} T_F\right] .$$

The running coupling constant $\bar{g}(Q^2)$ satisfies

$$\frac{\partial \bar{g}(Q^2)}{\partial(\ln(Q^2/\mu^2))} \equiv \beta(\bar{g}(Q^2))$$

and is approximately

$$\bar{g}^2(Q^2) \simeq \frac{g^2}{1 + \frac{1}{2}\beta_0 g^2 \ln(Q^2/\mu^2)} \,.$$

The anomalous dimension matrix of twist-two operators in the operator product expansion, appropriate to the $n$th moment of $W(x)$ is

$$\Gamma_{n-1} = \begin{pmatrix} -\gamma_{n-1}^{NS} & -\gamma_{n-1}^{QG} \\ -\gamma_{n-1}^{GQ} & -\gamma_{n-1}^{GG} \end{pmatrix} ,$$

with

$$-\gamma_{n-1}^{NS} = \lambda C_F f_n \,,$$

$$f_n = -\frac{1}{2}\left[1 - \frac{2}{(n+1)(n+2)} + 4 \sum_{j=2}^{n+1} \frac{1}{j}\right] ,$$

$$-\gamma_{n-1}^{QG} = 2\lambda T_F \left[\frac{n^2 + 3n + 4}{(n+1)(n+2)(n+3)}\right] ,$$

$$-\gamma_{n-1}^{\mathrm{GQ}} = \lambda C_{\mathrm{F}}\left[\frac{n^2+3n+4}{n(n+1)(n+2)}\right],$$

$$-\gamma_{n-1}^{\mathrm{GG}} = \tfrac{1}{2}\lambda C_{\mathrm{G}}\left[\frac{1}{3}+\frac{4}{n(n+1)}+\frac{4}{(n+2)(n+3)}-4\sum_{j=2}^{n+1}\frac{1}{j}\right]-\tfrac{1}{2}\lambda\left[\tfrac{4}{3}T_{\mathrm{F}}\right].$$

Our $Z$ factors are defined relative to *renormalized full* propagators and *one particle irreducible* vertices normalized to their bare value at euclidean points characterized by mass $\mu$:

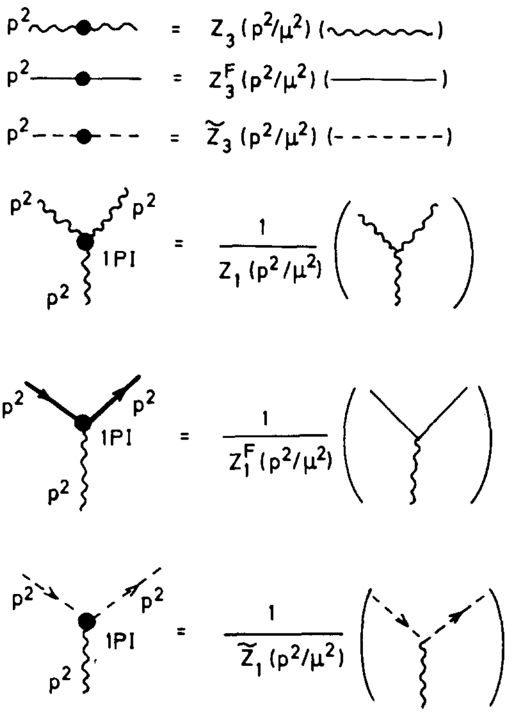

(A.2)

neglecting induced terms in the vertices with different tensor properties (which are negligible asymptotically) and setting $m = 0$.

In our stagnant Feynman gauge, these functions satisfy renormalization group equations like (A.1) with the appropriate field anomalous dimensions expressed *in the stagnant Feynman gauge* (which are the same as in ordinary Feynman gauge in $O(g^2)$) and *without* the usual "gauge drift" term $\delta\partial/\partial\alpha$. Thus, e.g., $Z_3(P^2/\mu^2)$ satisfies

$$\left[\frac{-\partial}{\partial(\ln(P^2/\mu^2))}+\beta\frac{\partial}{\partial g}-2\gamma_{\mathrm{A}}\right] Z_3(P^2/\mu^2)=0\,; \qquad \text{(A.3)}$$

with

$$\gamma_A = -\tfrac{1}{4}\lambda[-\tfrac{5}{6}C_G + \tfrac{4}{3}T_F]$$

and solution

$$Z_3(P^2/\mu^2) = \left(\frac{\bar{g}^2(p^2)}{g^2}\right)^{4\gamma_A/g^2\beta_0} ; \qquad \text{(A.4)}$$

$Z_3^F$ satisfies (A.3) with $\gamma_F = -\tfrac{1}{4}\lambda C_F$, etc.

The $Z$'s satisfy the identity

$$\frac{[Z_3(p^2)]^3}{[Z_1(p^2)]^2} = \frac{[Z_3^F(p^2)]^2\, Z_3(p^2)}{[Z_1^F(p^2)]^2} = \frac{\bar{g}^2(p^2)}{g^2} \qquad \text{(A.5)}$$

and the Slavnov-Taylor identities

$$\frac{Z_3(p^2)}{Z_1(p^2)} = \frac{Z_3^F(p^2)}{Z_1^F(p^2)} = \frac{\tilde{Z}_3(p^2)}{\tilde{Z}_1(p^2)} . \qquad \text{(A.6)}$$

### A.4. Infrared-divergent radiation factors

Associated with *real* gluon radiation from an *incoming quark* line is the factor

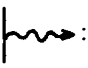 $$: r_n = \int_0^1 dy\, y^n \frac{1+y^2}{1-y} ;$$

$r_0$ is appropriate to an *outgoing quark* line.

Associated with *virtual* gluon radiation (summed up with Ward identities) from quark lines (incoming or outgoing) is

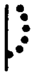 $$: v = \int_0^1 dy \frac{-2y}{1-y} .$$

Associated with *real* gluons from an *incoming gluon* line is

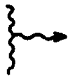 $$: \rho_n = \int_0^1 dy\, 2y^n \quad \frac{y}{1-y} + \frac{1-y}{y} + y(1-y) \quad ,$$

($\rho_0$ for outgoing gluons) and for *virtual* radiation

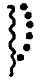 $$: \nu = -\int_0^1 dy \quad \frac{2-y}{y} + \frac{1+y}{1-y} \quad .$$

Real and virtual combine to form the infrared-finite factors

$$r_n + v = \frac{-1}{\lambda C_F}[\gamma_{n-1}^{NS} + 2\gamma_F] ,$$

$$\rho_n + \nu = \frac{-1}{\lambda C_G}\,[\gamma^{GG}_{n-1} + 2\gamma_A]\ .$$

At this point we also list the *finite* factors (used in sect. 6) associated with (i) quark emission from a gluon:

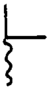

$$: \int_0^1 dy\, y^n [2 - 4y(1-y)] = \frac{2n^2 + 6n + 8}{(n+1)(n+2)(n+3)}$$

$$= \frac{-1}{\lambda T_F}\,\gamma^{QG}_{n-1}\ ;$$

(ii) quark emission from a quark:

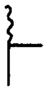

$$: \int_0^1 dy\, y^n\ \ y + \frac{2(1-y)}{y} = \frac{n^2 + 3n + 4}{n(n+1)(n+2)}$$

$$= \frac{-1}{\lambda C_F}\,\gamma^{GQ}_{n-1}\ .$$

## References

[1] C.H. Llewellyn Smith, Acta Phys. Austriaca, Suppl. XIX (1978) 331.

[2] Yu.L. Dokshitser, JETP (Sov. Phys.) 46 (1977) 641;
Yu.L. Dokshitser, D.I. D'Yakonov and S.I. Troyan, Inelastic processes in quantum chromodynamics, Proc. 13th Leningrad Winter School (1978) [SLAC TRANS-183].

[3] V.N. Gribov and L.N. Lipatov, Sov. J. Nucl. Phys. 15 (1972) 438, 675.

[4] D. Amati, R. Petronzio and G. Veneziano, Nucl. Phys. B140 (1978) 54; B146 (1978) 29;
A.V. Efremov and A.V. Radyushkin, Dubna preprints E2-11535, 11725, 11726, 11849 (1978);
W.R. Frazer and J.F. Gunion, Phys. Rev. D19 (1979) 2447;
J. Frenkel, M.J. Shailer and J.C. Taylor, Nucl. Phys. B148 (1979) 228;
Y. Kazama and Y.-P. Yao, Phys. Rev. Lett. 41 (1978) 611; Phys. Rev. D19 (1979) 3111; D19 (1979) 3121;
A.V. Radyushkin, Phys. Lett. 69B (1977) 245;
W.J. Stirling, Nucl. Phys. B141 (1978) 311; B145 (1978) 477;
C.T. Sachrajda, Phys. Lett. 76B (1978) 100; 73B (1978) 185.

[5] G. Sterman and S. Weinberg, Phys. Rev. Lett. 39 (1977) 1436.

[6] H.D. Politzer, Nucl. Phys. B122 (1977) 237; Phys. Lett. 70B (1977) 430.

[7] R.K. Ellis, H. Georgi, M. Machacek, H.D. Politzer and G.G. Ross, Phys. Lett. 78B (1978) 281; Nucl. Phys. B152 (1979) 285;
S. Gupta and A.H. Mueller, Phys. Rev. D20 (1979) 118;
A.H. Mueller, Phys. Rev. D18 (1978) 3705;
G. Sterman and S. Libby, Phys. Rev. D18 (1978) 3252; 4737; Phys. Lett. 78B (1978) 618.

[8] T. Kinoshita, J. Math. Phys. 3 (1962) 650;
T.D. Lee and M. Nauenberg, Phys. Rev. 133 (1964) 1549.

[9] S. Coleman and R.E. Norton, Nuovo Cim. 38 (1965) 438.
[10] C.H. Llewellyn Smith, Oxford preprint, Nucl. Phys. B, to be published.
[11] A. Sugamoto, Phys. Rev. D16 (1977) 1065.
[12] G. Altarelli and G. Parisi, Nucl. Phys. B126 (1977) 298.
[13] A.B. Carter, Oxford University thesis (1979).
[14] G. 't Hooft and M. Veltman, Nucl. Phys. B50 (1972) 318.
[15] C. Becchi, A. Rouet and R. Stora, Ann. of Phys. 98 (1976) 287.
[16] R.A. Brandt, Nucl. Phys. B116 (1976) 413.
[17] J.C. Taylor, Nucl. Phys. B33 (1971) 436;
A.A. Slavnov, Theor. Math. Phys. 10 (1972) 99.
[18] J. Kogut and L. Susskind, Phys. Rev. D9 (1974) 697, 3391.
[19] J. Ellis, M.K. Gaillard and G.G. Ross, Nucl. Phys. B111 (1976) 253 (E: B130 (1977) 516).
[20] E. Floratos, CERN preprint TH2661 (1976); Nuovo Cim. 43A (1978) 241.
[21] K.H. Craig and C.H. Llewellyn Smith, Phys. Lett. 72B (1978) 349.
[22] C.H. Llewellyn Smith, Phys. Lett. 79B (1978) 83.
[23] J.D. Bjorken and S.D. Drell, Relativistic quantum mechanics (McGraw-Hill, 1964).